

Frontopolar cortex shapes brain network structure across prefrontal and posterior cingulate cortex

Matthew Ainsworth^{a,b,*}, Zhemeng Wu^{a,c,*}, Helen Browncross^a, Anna S. Mitchell^a, Andrew H. Bell^{a,b}, Mark J. Buckley^a

^a Department of Experimental Psychology, University of Oxford, Oxford OX1 3SR, United Kingdom

^b MRC Cognition and Brain Sciences Unit, University of Cambridge, 15 Chaucer Road, Cambridge, United Kingdom

^c Department of Psychology (Scarborough), University of Toronto, Toronto, ON, Canada

ARTICLE INFO

Keywords:

Frontopolar cortex
Resting-state connectivity
Prefrontal cortex
Macaque
fMRI

ABSTRACT

Primate frontopolar cortex (FPC), occupied by area 10, sits atop a functional hierarchy of prefrontal cortical regions, yet little is known about its involvement in wider cortical networks. Here we examined resting-state-functional-connectivity (rsfc) in rhesus monkeys with intact or lesioned FPC to identify cortical regions associated with FPC. We present a network of FPC-specific regions of interest (ROIs), whose connectivity was affected by lesion of FPC but not by lesion of neighbouring prefrontal cortex (principal sulcus). This network comprised 'core ROIs' with direct anatomical connections to FPC, located in ventrolateral prefrontal cortex, posterior cingulate cortex, and superior temporal gyrus, and 'peripheral ROIs' well connected to the core network. We further show that the principle effect of a lesion to FPC was to cause a profound disturbance of the functional connectivity of posterior cingulate and ventrolateral prefrontal cortex. We therefore suggest that FPC, posterior cingulate and ventrolateral prefrontal cortex comprise a network of interacting cortical areas whose interactions may be critical for mediating the contribution of FPC to decision making.

Abbreviations: FPC, frontopolar cortex; PS, principal sulcus; vlPFC, ventrolateral prefrontal cortex; PCC, posterior cingulate cortex; STG, superior temporal gyrus; NHPs, non-human primates; rsfc, resting state functional connectivity; ROI, region of interest; TMS, transcranial magnetic stimulation; MRI, magnetic response imaging; SVD, singular value decomposition; FDR, false discovery rate; A1, auditory cortex area 1; AIP, anterior intraparietal area; Area 1, somatosensory area 1; Area 2, somatosensory area 2; Area 3a, somatosensory area 3a; Area 3b, somatosensory area 3b; Area 4 C, premotor area 4 C; Area 5 V, somatosensory area 5 V; Area 6Val, ventral premotor area subdivision al; Area 6Vam, ventral premotor area subdivision am; Area 6Vb, ventral premotor area subdivision b; Area 7b, visual area 7b; Area 7op, parietal operculum; Area 7 t, transitional area 7; Area 8As, area 8 subdivision As; Area 8Ac, area 8 subdivision Ac; Area 12o, area 12 orbital subdivision; Area 12r, area 12 rostral subdivision; Area 13 l, area 13 lateral subdivision; Area 18 V2, visual area 2; Area 23, posterior cingulate area 23; Area 23a, posterior cingulate area 23a; Area 23b, posterior cingulate cortex area 23b; Area 29a-c, retrosplenial cortex area 29a-c; Area 29d, retrosplenial cortex area 29d; Area 30, retrosplenial cortex area 30; Area 31, cingulate area 31; Area 35 PHT00, area 35 of perirhinal cortex (PHT atlas); Area 36r, area 36 of perirhinal cortex (rostral subregion); Area 46 v, area 46 (ventral subdivision); Area 45, prefrontal area 45; DP, dorsal prelunate area; EOI, entorhinal cortex; Frontal 23, posterior cingulate frontal area 23; FST, floor of superior temporal area; GranInsula, granular insula cortex; GustCtx LV00, gustatory cortex (LV00 atlas); GustCtx PHT00, gustatory cortex (PHT atlas); IPa, superior temporal sulcus fundus; InsPro, proisocortex; LIPd, lateral intraparietal area (dorsal); LOP, lateral occipital parietal area; MSTda, medial superior temporal area (subdivision da); MSTdp, medial superior temporal area (subdivision dp); MT, middle temporal area; Parietal 23, posterior cingulate parietal area 23; PiriCtx, piriform cortex; PECg, parietal area PE, cingulate part; PGM, parietal area PE, medial part; PIP, posterior intraparietal area; PO, parieto-occipital area; PrCO, precentral opercular area of the frontal operculum; Retroinsula, retroinsula cortex; S2, somatosensory area 2 (complex); ST2g, superior temporal sulc area 2, gyral; ST2s, superior temporal sulc area 2; TLR area 36R, area 36 of perirhinal cortex (rostral subregion); TAA, superior temporal gyrus area; TEa, superior temporal sulcus lateral bank; TE1, temporal area TE1; TE1–3d, subdivisions TE1, TE2, and TE3; Tpt, temporo-parietal area; TPOi, superior temporal sulcus dorsal bank (intermediate); TPOR, superior temporal sulcus dorsal bank (rostral); Ts, superior temporal cortex; VIPl, ventral intraparietal area (lateral subdivision); VIPm, ventral intraparietal area (medial subdivision); V3A, visual area 3a; V4, visual area 4; V4ta, V4 transitional area (anterior); V4tp, V4 transitional area (posterior); VP, ventral posterior area; OFC, orbitofrontal Cortex; STS, superior temporal sulcus; Area 7a, visual area 7a; Area 6DR, premotor area (rostral dorsal subdivision) Area 6M, premotor area (medial subdivision); Area 12l, area 12 lateral subdivision; Area 13a, area 13 anterior subdivision; Area 13b, frontal area 13b; Area 14r, area 14 rostral subdivision; Area 24b, cingulate area 24b; INSai, agranular insular cortex (area ai); INSam, agranular insular cortex (area am); IPS, intraparietal sulcus; ProSt, prostriata area; PaS, parasubiculum; PreS, presubiculum; LIPv, lateral intraparietal area (ventral); MSTm, medial superior temporal area (subdivision m) ST1, superior Temporal sulcus area 1; TPPai, temporo-parietal periallocortex; TPPro, temporo-parietal proisocortex; ProM, proisocortical motor cortex.

* Corresponding authors at: Department of Experimental Psychology, University of Oxford, Oxford OX1 3SR, United Kingdom.

E-mail addresses: matthew.ainsworth@psy.ox.ac.uk (M. Ainsworth), zhemeng.wu@utoronto.ca (Z. Wu).

<https://doi.org/10.1016/j.pneurobio.2022.102314>

Received 24 December 2021; Received in revised form 8 April 2022; Accepted 1 July 2022

Available online 4 July 2022

0301-0082/© 2022 The Authors. Published by Elsevier Ltd. This is an open access article under the CC BY license (<http://creativecommons.org/licenses/by/4.0/>).

1. Introduction

Frontopolar cortex (FPC) is occupied by area 10, a cytoarchitectonic area exclusive to primates. Correlational neuroimaging studies have associated human FPC activities with a diverse range of higher-order cognitive functions. These include, but are not limited to, maintaining and integrating subgoals to fulfil outcomes (Badre and Wagner, 2004; Bunge et al., 2009; Christoff et al., 2003, 2001), explorative behaviour (Boorman et al., 2009; Daw et al., 2006), cognitive control (Nee and D'Esposito, 2017, 2016), cognitive branching (Koechlin et al., 1999), future planning (Burgess et al., 2011), prospective memory (Koechlin et al., 2000; Okuda et al., 2007, 2003), and memory awareness (Ryals et al., 2015; Yokoyama et al., 2010).

A recent interpretation of FPC function, based both upon the human neuroimaging literature as well as a combination of lesion and electrophysiological data from non-human primates (NHPs) proposed that FPC contributes to disengaging cognitive control from the current task and redistributing resources to other potential goals (Mansouri et al., 2017). Therefore, in direct contrast to more posterior parts of the prefrontal cortex that work together to facilitate efficient 'exploitation' of reward opportunities, according to this hypothesis FPC is essential for mediating 'exploration'. Such an interpretation is consistent with recent findings from a transcranial magnetic stimulation (TMS) study in which the authors observed a specific decrease in directed, but not random, exploration after targeting human lateral FPC (Zajkowski et al., 2017).

Irrespective of whether FPC is essential for controlling explorative behaviour, or in facilitating one or more of the many alternatives listed above, its contribution to cognition presumably involves interactions with a number of posterior brain regions. From detailed anatomical tracing studies, we know that FPC has a pattern of robust reciprocal connections to other cortical areas distinct from other prefrontal areas. FPC has extensive connections within prefrontal cortex; with strong connections to areas of both ventromedial (areas 14 and 13) and lateral prefrontal cortex (areas 9 and 12). In addition, FPC is well connected to medial prefrontal regions including anterior cingulate cortex, as well as posterior cingulate cortex (Markov et al., 2014; Petrides and Pandya, 2007). Within the temporal lobe, FPC has robust bidirectional connections with a number of regions, including superior temporal gyrus auditory areas (including primary auditory cortex and TPO and TAa) dorsally, and ventrally with a number of supramodal areas of medial temporal cortex including areas TH, TF, entorhinal, and temporal polar cortex (Markov et al., 2014; Petrides and Pandya, 2007). FPC does have some connections with unimodal areas but its connections to occipital cortex and visual inferotemporal cortex are light in comparison, as are connections with parietal cortex (Markov et al., 2014; Petrides and Pandya, 2007).

Despite detailed knowledge of the anatomical connections which link FPC to the rest of the brain, our understanding of functional communication between FPC and these posterior cortical regions is less developed. To-date few studies have examined the connectivity of FPC during cognitive testing. Whilst those few that have, understandably focus on the modulation of connectivity between FPC and specific regions-of-interest (ROIs). For example, Sakai and Passingham demonstrated that connectivity between FPC and both premotor and ventrolateral prefrontal cortex varied depending on the intended cognitive operation held in working memory (Sakai and Passingham, 2006). Similarly, Boorman et al. (2009) identified an increase in correlation between activity in FPC and ROIs in parietal cortex immediately before behavioural switches.

Our lack of knowledge about how FPC interacts with other cortical regions is particularly glaring given recent advances, facilitated by whole-brain neuroimaging, which increasingly emphasise the importance of networks of regions, commonly co-activated in response to certain features or tasks. Two examples include the widely studied frontoparietal network involved in control of spatial-attention (Corbetta, 1998; Corbetta and Shulman, 2002; Nobre, 1997), and the more

recently described cortical social network in macaques, activated when viewing social interactions (Ainsworth et al., 2021; Sliwa and Freiwald, 2017). However, the role of FPC within wider cortical networks, either at rest or during task performance is unclear. For example, although FPC is included in the default-mode network in humans (Raichle et al., 2001) it is absent from the comparable network observed in macaques (Mantini et al., 2011). In addition, despite the association of FPC activation with an extensive list of cognitive functions (see above), it is not considered to be a constituent of the multi-demand network, (a group of regions thought to be commonly activated in response to cognitive challenge) in either humans (Duncan, 2010; Fedorenko et al., 2013) or macaques (Mitchell et al., 2016). Furthermore, although several studies have examined the connectivity of FPC in both human and macaques they have primarily sought to find similarities between the two species (Neubert et al., 2015, 2014). Therefore, by necessity the authors focused on examining connectivity from FPC to a limited sub-selection of ROIs common to both species, rather than to the whole brain.

Understanding the functional connections of FPC to the wider brain is an essential step towards identifying the contribution of FPC to cognition and accordingly, advancing our understanding of functioning of the wider prefrontal cortex. Here we took a combined causal (lesion) and correlational (fMRI) approach to identify the necessity of FPC for maintaining posterior network connectivity. Specifically, we combined circumscribed FPC lesions in macaques with analyses of whole brain resting-state functional connectivity (rsfc) to (i) identify a network of regions connected to FPC, and to (ii) explore changes in connectivity within this network after a lesion to FPC. To assess specificity of the effect of FPC lesions per se we used an iterative whole-brain analysis to identify regions affected by FPC lesions, before dissociating the changes in connectivity associated with FPC lesions from those associated with lesions of principal sulcus (PS), wherein cortex on both banks of the PS were lesioned. Based on our analyses we present a network of FPC-specific ROIs. This network comprised 'Core ROIs' with direct anatomical connections to FPC, located in ventrolateral prefrontal cortex, posterior cingulate cortex, and superior temporal gyrus, and 'Peripheral ROIs' well connected to the core network. We show that the principle effect of a lesion to FPC is to disturb functional connectivity of posterior cingulate and ventrolateral prefrontal cortex. Based on these findings we suggest that these areas may form the basis of a network essential to the function of FPC. Therefore, understanding the interactions between these areas, during behaviour may provide greater insight into the contribution of FPC to decision making.

2. Results

We collected resting state fMRI data and structural scans under anaesthesia from a total of 30 animals allocated to our four experimental groups. To identify a network of regions associated with FPC we compared functional connectivity (defined as pairwise correlation calculated from BOLD fMRI) between 256 cortical areas of the cytoarchitectonic (CC) atlas (van Essen et al., 2012), in animals with and without lesions of the FPC. In addition, we examined differences in functional connectivity between two further experimental groups, before and after lesion of PS.

Changes in cortex-wide functional connectivity associated with lesions of FPC were identified by differences between the two groups: animals scanned approximately 8 weeks after FPC lesion (FPC-lesion group, three animals) and a control group of animals with intact FPC (FPC-control group, 13 animals). All three FPC-lesion animals received complete bilateral aspiration lesions of the FPC (Fig. 1B) with a surgical intention of minimising underlying white matter damage.

To determine if changes in functional connectivity were specific to the bilateral and relatively circumscribed FPC lesions, or might instead be undifferentiated from any general frontal cortical insult, such as to posteriorly adjacent prefrontal cortex (under which some of the same white matter tracts run), we also explored the impact of unilateral PS

lesions on functional connectivity in two further groups: Animals scanned approximately 6 weeks after PS lesion (PS-lesion group, two animals) and animals with intact PS (PS-control group, 12 animals). The two PS-lesion animals received unilateral aspiration lesions of the left PS (Fig. 1C).

2.1. Changes of functional connectivity after lesion of FPC and PS

To localise functional connections affected by lesions of FPC, we conducted a standard assumption-free nonparametric permutation test comparing inter-area correlation strengths in the FPC-control and FPC-lesion groups. This test revealed 466 functional connections which were significantly different between control animals and the FPC-lesion animals (two-tailed permutation test, $p < 0.05$). These significant functional connections linked 85 of the cortical regions from the Van Essen cytoarchitectonic parcellation, that we henceforth refer to as non-specific ROIs affected by lesion of FPC. Accordingly, Fig. 2A.ii shows just the connections between these 85 ROIs. These ROIs included a number of regions within the frontal lobe as well as more posterior areas located

within the parietal and temporal lobes. ROIs identified in the frontal lobe included areas of the orbitofrontal (areas 12o and 13 l), dorsolateral (46 v), ventrolateral (area 46 v, area 12, and area 12r) and pre-motor cortex (area 6), as well as insular and gustatory cortex. Within the parietal lobe, ROIs included areas of posterior cingulate cortex and regions both anterior (areas 2,3 and 5 v) and posterior to the intraparietal sulcus (LIP, AIP, and area 7). Finally, a number of ROIs were located within the temporal and occipital lobes (including V2 and V4, MT, FST, and MST, see Table S1 for full list and MRI coordinates of FPC non-specific ROIs).

By contrast, a nonparametric permutation test examining differences between the PS-control and PS-lesion groups revealed 61 functional connections significantly affected by the lesion of the PS (two-tailed permutation test, $p < 0.05$). These significant functional connections linked 32 distinct cortical ROIs (mean correlation matrices between these 32 non-specific ROIs shown in Fig. 2B.ii, see Table S2 for full list and MRI coordinates of PS ROI's).

The FPC and PS networks clearly overlapped to a degree. Direct comparison of these sets of distinct ROIs identified by the two

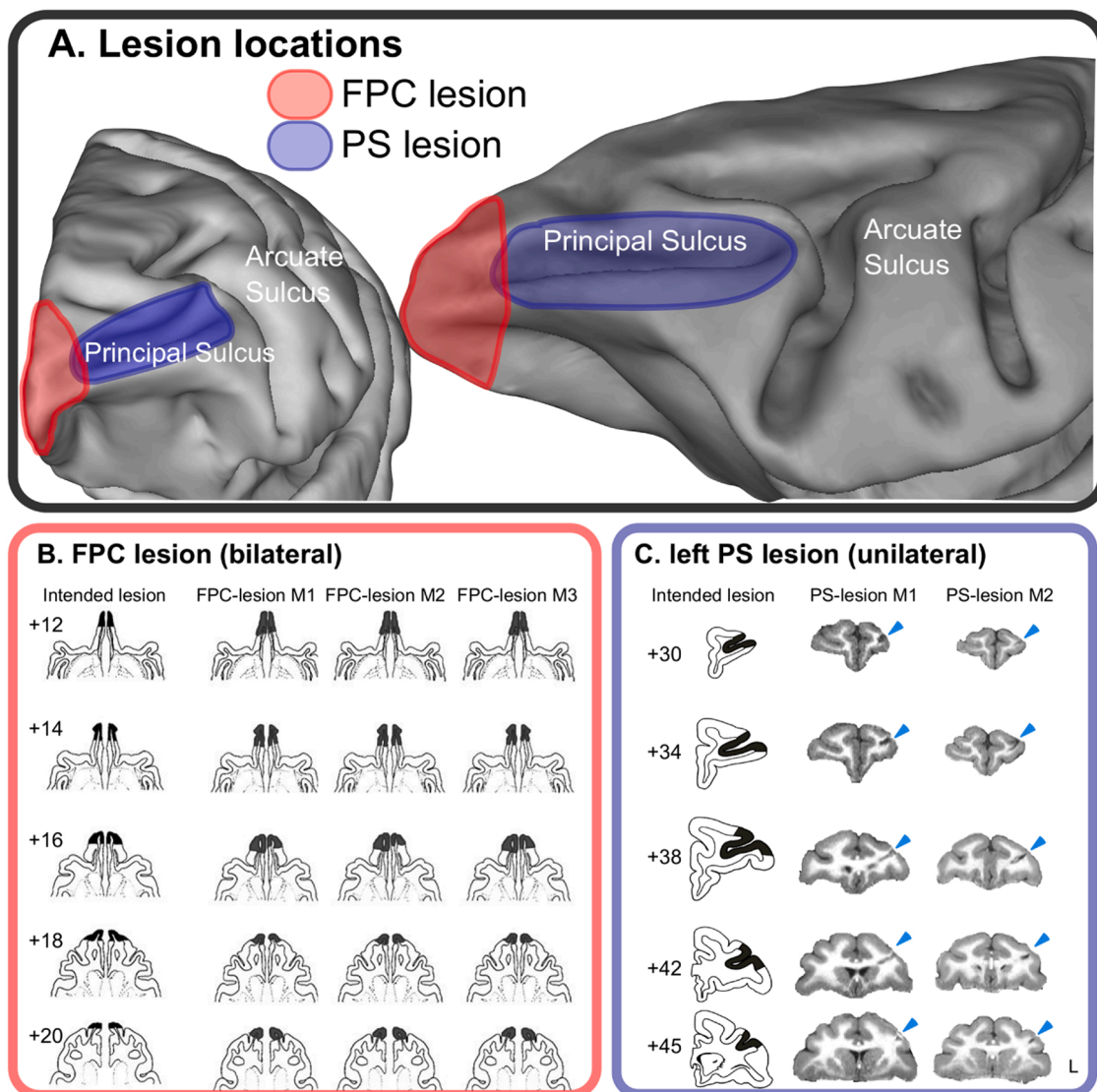
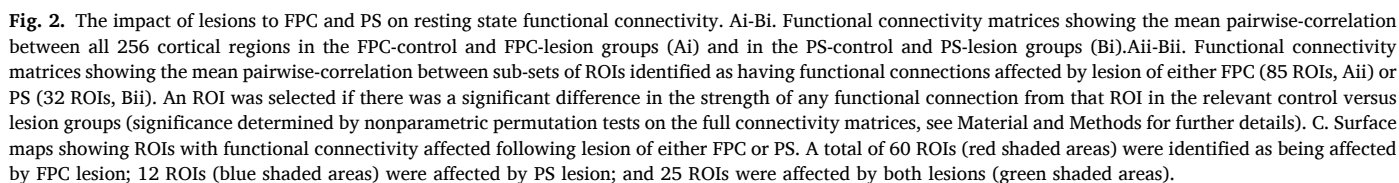


Fig. 1. Intended and actual extent of the bilateral FPC lesion and unilateral left hemisphere PS lesion. **A.** Intended extent of lesion locations of FPC (red) and PS (blue) in drawings of the inflated macaque brain. **B.** Drawings of horizontal sections through macaque prefrontal cortex the intended extent of the FPC-lesion and the actual lesion extent in the three FPC-lesioned animals. **C.** Drawings of coronal sections through macaque prefrontal cortex showing the intended lesion extent of the unilateral PS-lesion and structural fmri showing the actual lesion in the two PS-lesion animals. All numbers represent the approximate distance in millimeters relative to the interaural line. Detailed descriptions of lesion extents from all animals have been published elsewhere in detail (Ainsworth et al., 2018; Boschini et al., 2015).



(see Fig. 2C). ROIs that appeared to be affected in this way by both FPC and PS lesion included areas of gustatory and insular cortex as well as premotor cortex, and regions of parietal cortex anterior of IPS.

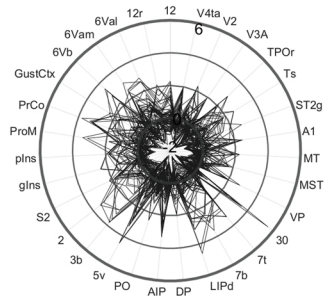
This overlap between ROIs limited our ability to infer the specific

changes in connectivity associated with FPC lesion, and in turn a specific network of regions with notable functional connections to FPC. Therefore, we conducted further analyses to dissociate changes in connectivity caused by the two lesions. Firstly, differences between control and lesion groups were visualised by generating connectivity fingerprints (Mars

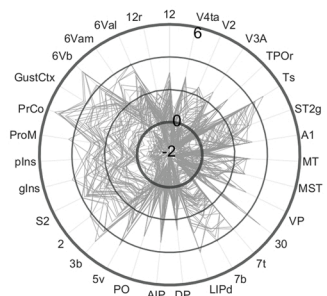
et al., 2011) for each of the aforementioned ROIs. Among these 85 ROIs, 31 of them were identified bilaterally (noting that Gustatory LV00 and PHT00 were combined to form one Gustatory cortex ROI). The connectivity fingerprints were visualised as polar plots (Fig. 3) in which the 31 bilaterally occurring ROIs (unilaterally occurring ROIs were not

A. Bilateral lesion of FPC

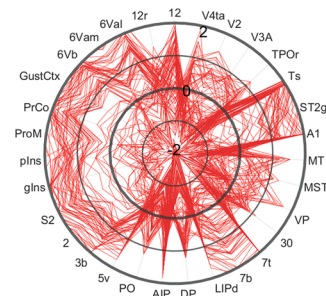
i. FPC-control



ii. FPC-lesion

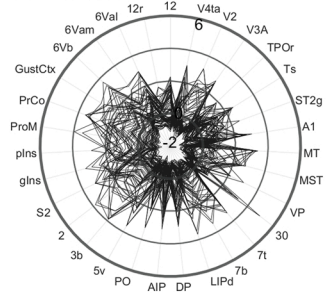


iii. Difference

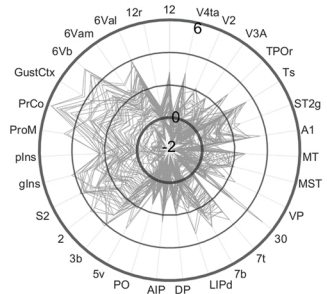


B. Unilateral lesion of Left PS

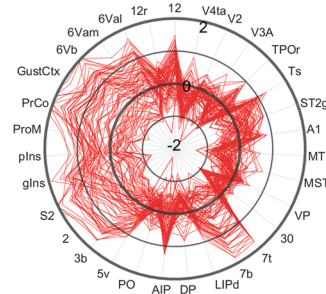
i. PS-control



ii. PS-lesion

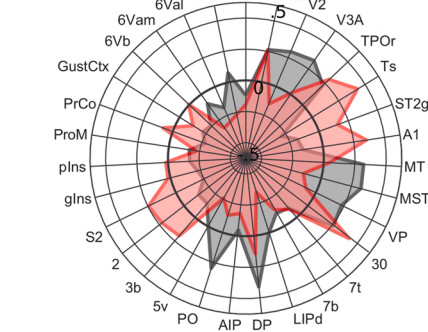


iii. Difference

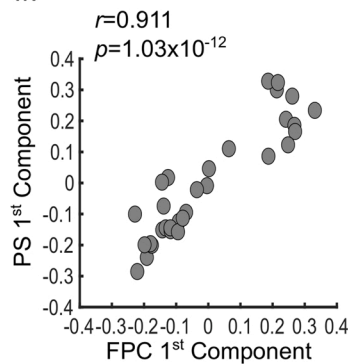


C. FPC lesion SVD components

i.

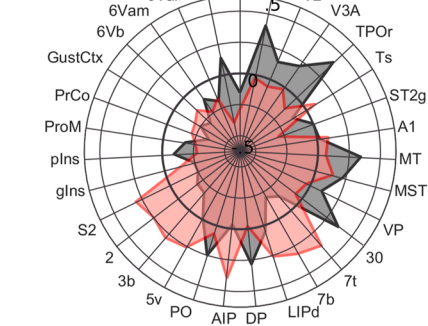


ii.



D. PS lesion SVD components

i.



ii.

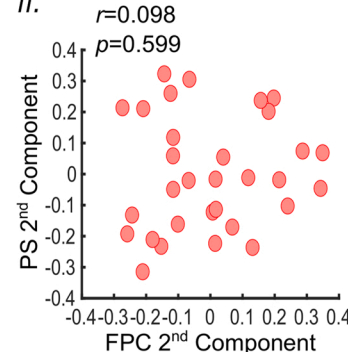


Fig. 3. Specific changes in functional connectivity after lesion of FPC and PS revealed by connectivity fingerprints and singular value decomposition (SVD). A. Functional connectivity fingerprints in FPC-control (Ai) and FPC-lesion groups (Aii). B. Functional connectivity fingerprints in PS-control (Bi) and PS-lesion groups (Bii). For all four polar plots each spoke on the plot depicts connectivity to one labelled ROI (i.e., one spoke for each of the 31 significant ROIs present bilaterally) with each circumferential line depicting the mean functional connectivity to these 31 bilateral ROIs from one of the 85 previously identified ROIs (hence 85 points are plotted per spoke). Difference of connectivity fingerprints between the FPC-control and FPC-lesion groups is depicted in (Aiii), and difference of connectivity fingerprints between the PS-control and PS-lesion groups is depicted in (Biii). Ci-Di. The first two components (1st and 2nd in grey and red outlines respectively) revealed by singular value decomposition of FPC connectivity fingerprints (Ci) and PS connectivity fingerprints (Di). See Materials and Methods for details of the SVD analysis. Cii-Dii. The first component (grey coloured dots) in FPC and PS showed a positive correlation (Cii) while the second component (red coloured dots) in FPC and PS demonstrated no linear relationship (Dii).

included in the analysis) formed the 'spokes' on the polar plot and their strength of correlation to the previously identified 85 ROIs in the aforementioned non-parametric analyses were plotted as 85 separate (hence overlapping) lines on each polar plot. The identical approach was used to generate the fingerprints for the PS lesion experimental groups (Fig. 3B).

Comparison of these connectivity fingerprints (FPC-control vs. FPC-lesion, Fig. 3A.i & ii; and PS-control vs. PS-lesion groups, 3B.i & ii, respectively) emphasised that the connectivity profiles varied greatly across all the 85 ROIs. This variance, and complexity within the data limited the conclusions that could be made from such connectivity fingerprints without further analysis. For example a number of post lesion fingerprints suggested both lesions were associated with increased connectivity to areas of premotor, gustatory, and insular cortex as well as anterior (namely areas S2, 2, and 3b) and posterior parietal regions (LIPd and area 7). However, close inspection of difference fingerprints, directly visualizing the difference in connectivity between the control and lesion groups (Fig. 3A.iii & B.iii for FPC and PS lesions, respectively) revealed that this increase occurred for some but not all of the 85 ROIs. Indeed connectivity to premotor, gustatory, and insular cortex decreased for some ROIs after both lesion of FPC and PS. Furthermore, there were no clear changes in connectivity to visual areas in temporal and occipital cortex (e.g., V2, V3A, TPOr) and retrosplenial cortex (e.g., area 30) associated with either lesion. This complicated pattern of fingerprints justified further analysis to distinguish significant changes related to FPC and PS lesions.

Given this complexity, we carried out a singular value decomposition (SVD) analysis on the difference fingerprints calculated from FPC control and lesion groups and PS control and lesion groups, separately. In this analysis the matrices of difference fingerprints (each matrix contained one difference fingerprint for each of the 85 ROIs) were decomposed into a series of components. For each lesioned area (FPC and PS), each of these components described a pattern of changes in connectivity between the respective control and lesion groups group difference change in connectivity, which accounted for the greatest proportion of variance remaining in the matrix (see Materials and Methods for further details).

The changes in connectivity described by the first two SVD components accounted for the most commonly occurring changes in connectivity associated with both lesions. Taken together these two components explained over 80% of the variance in the change in connectivity across all 85 ROIs, associated with lesion of either FPC or PS.

For both the FPC and PS lesion, the first SVD component explained the majority of the variance associated with each lesion (86 % and 68 % of the variance of the FPC-lesion and PS-lesion difference fingerprints, respectively). In addition, the first SVD component for the FPC-lesion and for the PS-lesion had remarkably similar patterns of connectivity (black outlines in Fig. 3C.i and 3D.i). These two components were characterised by increased connectivity to areas in the posterior parietal areas of the IPS (areas PO, DP), retrosplenial cortex (area 30), temporal (areas MST, MT and TPOr) and occipital lobes (areas VP, V2, V3A and V4ta). In addition, there was decreased connectivity to premotor cortex (areas 6Val, 6Vam and 6Vb), gustatory cortex, insular cortex (PrCo, ProM, proiso and granular insular cortex) and anterior parietal areas of the postcentral gyrus and sulcus (areas S2, 2 and 3b). Furthermore, these two components were strongly correlated (Pearson's $r = 0.911$, $p = 1.03 \times 10^{-12}$, Fig. 3C.ii), suggesting that this first component described changes in connectivity common to both the lesion of FPC and PS.

By contrast, the second SVD components explained a smaller proportion of the variance associated with each lesion (7% and 14% of the variance of the FPC-lesion and PS-lesion difference fingerprints, respectively) and described distinctly different patterns of connectivity. The second FPC-lesion component (red outlines in Fig. 3C.i) described a pattern with increased connectivity to anterior parietal areas of the IPS (areas S2, 2 and 3b), retrosplenial cortex (area 30), and superior

temporal areas (areas A1, St2g, Ts and TPOr), but decreased connectivity to ventrolateral prefrontal cortex (vlPFC, areas 12 and 12r), premotor areas (areas 6Val and 6Vam), gustatory cortex, posterior parietal areas of the IPS (areas PO, AIP, LIPd, 7b and 7t), and visual areas (areas VP, MST and V2). Although the pattern of connectivity described by the second PS-lesion component (red outlines in Fig. 3D.i) included decreased connectivity to vlPFC (areas 12 and 12r), premotor areas (areas 6Val, 6Vam and 6Vb) and gustatory cortex, it also included decreased connectivity to insular cortex (PrCo, ProM and proiso and granular insular cortex), retrosplenial cortex (area 30) and more visual areas (areas VP, V2, V3A and V4ta), and increased connectivity to both anterior (areas S2, 2, 3b and 5v) and posterior parietal areas (areas PO, AIP, LIPd, 7b and 7t). Direct comparison of the second FPC-lesion and PS-lesion components confirmed that they were not significantly correlated (Pearson's $r = 0.098$, $p = 0.599$, Figure. 3Dii).

2.3. Cortical regions affected by lesion of FPC

These data suggest that the two second SVD components identified from the previous analyses represent changes in connectivity, which were specific to the lesion of FPC and PS, rather than changes common to both lesions. Therefore, two further analyses were conducted to examine the specific effects of FPC lesions on network connectivity. Firstly, we carried out a whole-brain search to identify cortical regions in which lesions of FPC caused changes in connectivity that matched the corresponding second SVD component. To ensure this ROI selection was unbiased and avoid circular inference (i.e., to avoid including only ROIs identified in the previous permutation analysis), this analysis was carried out across the whole brain (with all 260 cortical regions included), using a leave one-out method (see Materials and Methods for details). Secondly, we used multi-dimensional scaling (MDS) to visualise the connectivity between these ROIs in control animals, and to examine changes in the relationship between these ROIs, after the lesion of FPC.

Whole brain analysis of the difference between the FPC-lesion and FPC-control groups (Fig. 4A) revealed 40 regions, henceforth referred to as FPC-specific-ROIs, (see Fig. 4B & Table S2 for a list of FPC-specific-ROIs), with difference fingerprints that fit the pattern of the second FPC-lesion SVD component significantly better than expected by chance (one-sided permutation test, $p < 0.05$, corrected for multiple comparisons using FDR).

Examination of functional connections between this network of 40 FPC-specific ROIs revealed a highly modular structure. The FPC-specific ROIs could be divided into five clusters; characterised by strong intra-cluster and weak inter cluster connectivity (clusters defined using k-means clustering, 90% of explained variance, Fig. 4C). Cluster 1 consisted primarily of posterior cingulate and retrosplenial cortex and included bilaterally medial parietal areas 23, 23a and 23b, area 29d and area 30. In addition, this cluster included left area 31, and PECg, as well as right retroinsula, area PGM, and area 29a-c. Cluster 2 consisted of regions of the temporal lobe. In the left hemisphere, cluster 2 was limited to the fundus (FST) and dorsal bank of the superior temporal sulcus, STS (area TAA). In the right hemisphere, cluster 2 was more extensive, extending from the dorsal bank of the STS (area TAA) to include regions of the superior temporal gyrus, STG (areas Ts, TPOi, TPOr and A1). Cluster 3 consisted of regions both anterior and posterior of the IPS. This cluster included area 7a, PO, and MSTdp in the left hemisphere as well as PIP, VIPI, VIPm, and MSTdp in the right hemisphere. Cluster 4 consisted exclusively of regions of the temporal pole. This cluster included area EOI, 36r and TE1 in the left hemisphere but was limited to area TE1 in the right hemisphere. Finally, cluster 5 comprised prefrontal cortex and included ventral premotor regions (area 6 Val) and area 12r in the left hemisphere as well as area 45 and 12r in the right hemisphere.

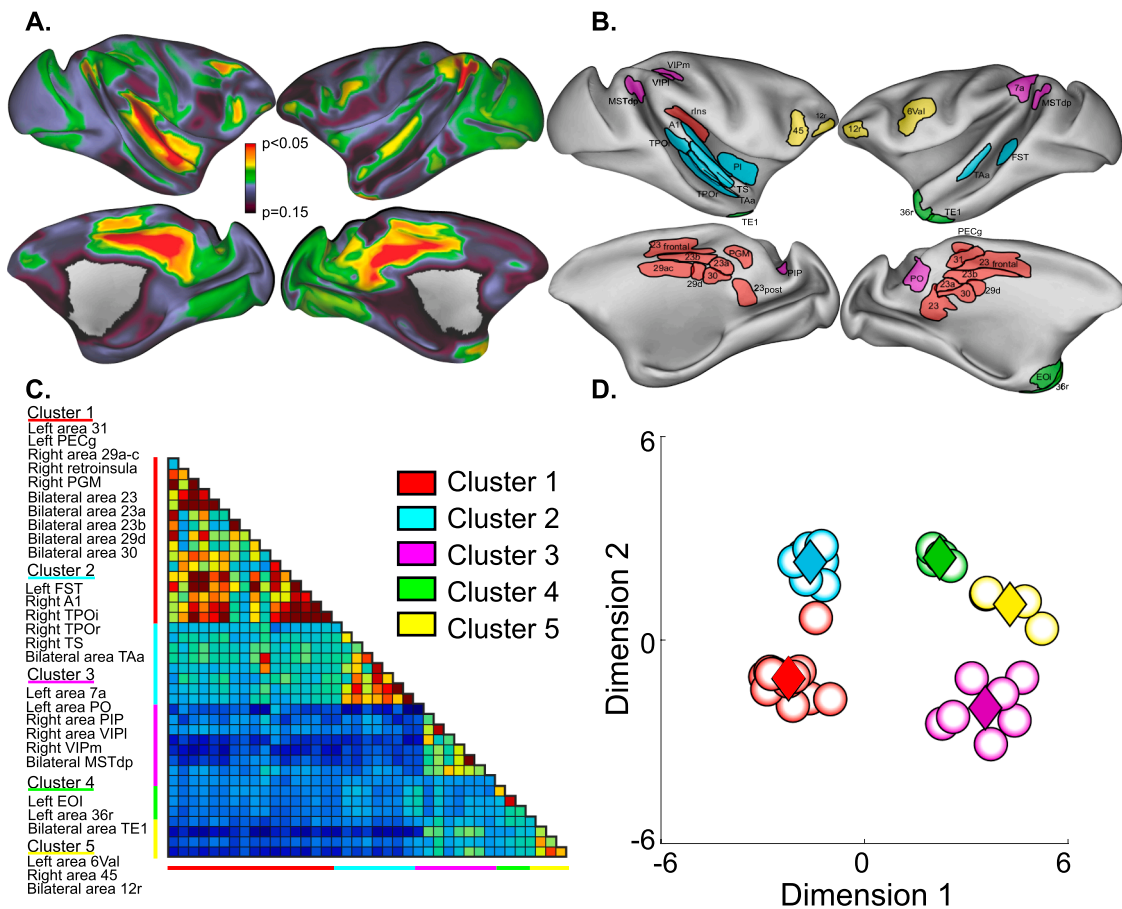


Fig. 4. The identification of the FPC-lesion specific network. A. Surface maps showing the results of a whole brain search for cortical regions with FPC-lesion induced changes in functional connectivity matching the second FPC-SVD component. A total of 40 FPC-specific-ROIs were identified in which changes in connectivity matched this SVD component better than expected by chance ($p < 0.05$ permutation test corrected for multiple comparisons with FDR, see Materials and Methods for full details of the whole brain search). Gray arrow indicates $p = 0.05$. B. Surface maps showing the cluster classes of FPC-specific-ROIs. FPC-specific ROIs were clustered based on their connectivity to FPC-specific ROIs and was defined by K-means clustering (into sufficient clusters to explain 90% of total variance). C. Functional connectivity matrix and multidimensional scaling plot calculated from pair-wise correlations between the FPC-specific-ROIs in the FPC-control groups. Within the connectivity matrix FPC-specific-ROIs are arranged by cluster (indicated by the colour bars to the bottom and left of the matrices), with a cluster-by-cluster breakdown of the FPC-specific ROIs shown to the left of the connectivity matrices. Within the MDS plot, FPC-specific-ROIs are represented as circles coloured according to cluster class, and are arranged such that the distance between ROIs corresponds to the similarity/dissimilarity between their patterns of connectivity. The centroid of each cluster, corresponding to the average connectivity of that cluster are depicted as coloured diamonds.

2.4. The relationship between anatomical and functional connectivity to FPC in FPC-specific ROIs

Our network of FPC-specific ROIs contained a diverse collection of cortical regions distributed across the brain. To better understand why these regions were affected by lesion of FPC we performed two further analyses. In these analyses we first examined each ROIs functional and anatomical connection to FPC before quantifying the importance of each ROI within our network.

To examine the functional and anatomical connectivity between FPC and our network of FPC-specific ROIs, we conducted a correlation analysis, comparing the functional and anatomical connection of all FPC-specific ROIs to FPC (Fig. 5A, anatomical connection data previously published in Markov et al., 2014). This analysis revealed a significant positive correlation between the strength of functional and anatomical connections from FPC-specific ROIs to FPC (Pearson's $r = 0.50$, $p = 0.001$, Fig. 5A). FPC-specific ROIs with stronger anatomical connections to FPC (e.g., areas TAa and 12r) also had strong positive functional connections to FPC, whilst those with weak anatomical connections in general had negative functional connections to FPC (e.g., areas MSTdp and PIP). In addition, several FPC-specific ROIs had moderate anatomical connections to FPC but weak or absent functional

connections to FPC (e.g., areas 23 and 30).

These data pose an interesting question: Why are so many cortical areas which are weakly connected to FPC affected by lesion of FPC? The simplest explanation for this phenomenon is that ROIs without connections to FPC are in turn strongly connected to ROIs that are connected to FPC. To test this hypothesis, we applied a threshold to the connections between our FPC-specific ROIs, to preserve only the strongest 3 connections of each ROI (see Material and Methods for details). This analysis revealed that suprathreshold connections predominately linked a small subset of ROIs. These “core” ROIs received a significantly greater number of suprathreshold connections, and therefore had a greater network degree, than expected by chance ($p < 0.05$, random permutation test with 1000 permutations, Fig. 5A & B).

These core ROIs all had moderate to strong connections to FPC according to the detailed tracing published by Markov et al. (Fig. 5A, Markov et al., 2014), and were confined to three locations: ventrolateral prefrontal cortex (e.g., area 12r and 45), the dorsal and ventral banks of the superior temporal gyrus, (e.g., A1, Ts, TAa and TPOr) and the posterior cingulate cortex (e.g., subdivisions of area 23, and area 30). Notably both superior temporal gyrus and posterior cingulate cortex are thought to be connected to FPC with direct fibre projections, the extreme capsule efferent fibre system and the cingulate fasciculus respectively

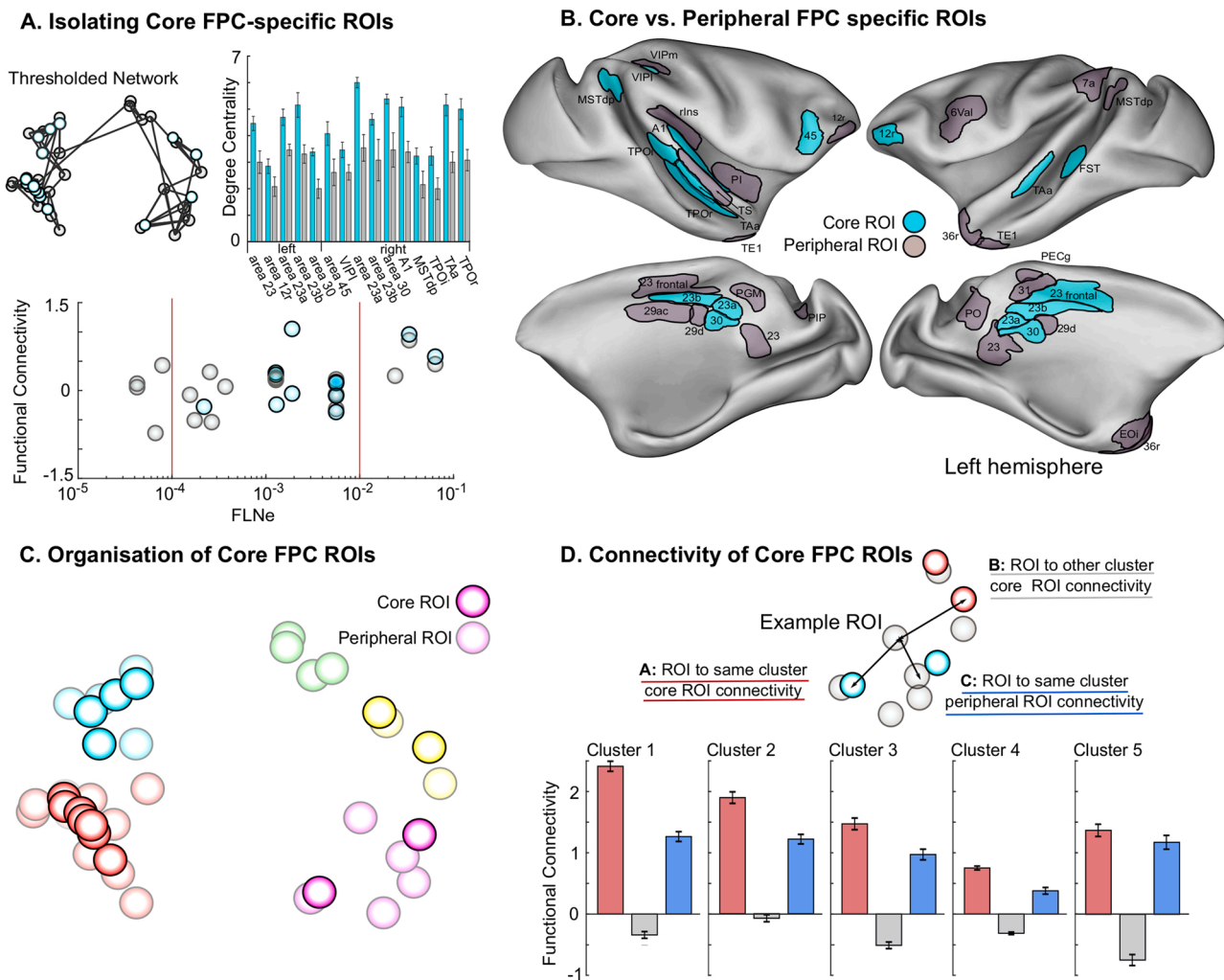


Fig. 5. The organisation of the FPC-specific network. **A.** Example network of FPC-specific ROIs after thresholding to include only the strongest 3 connections of each ROI. ROIs divided into “Core ROIs” with a greater number of connections to other ROIs than expected by chance shown (cyan), the remaining peripheral ROIs (grey, see Materials and Methods for details of the procedure for isolating core ROIs). The degree centrality, the total sum of all connections to an ROI, for all core ROIs (cyan) relative to chance (grey). Scatterplot showing the relationship between anatomical (extrinsic fraction of labelled neurons, FLNe, data taken from Markov et al., 2014) and functional connection strength to FPC for all FPC-specific ROIs, core and peripheral ROIs shown in cyan and grey respectively. **B.** Surface maps showing the anatomical location of core (cyan) and peripheral ROIs (grey). **C.** Multi-dimensional scaling plot showing the position of core (solid) and peripheral ROIs (transparent) within the network, and relative to the previously identified functional clusters. **D.** Bar charts showing the connectivity to within cluster core ROIs, to core ROIs from all other clusters and to peripheral ROIs within cluster. For each cluster, ROIs had significantly stronger connections to core ROIs within the same cluster compared to core ROIs from other clusters and peripheral ROIs. Note no core ROIs were found within cluster 4. Connectivity data shown calculated to core ROIs from cluster 5 (see Fig. S1 for a breakdown of the connectivity from ROIs in cluster 4 to core ROIs in other clusters).

(Petrides and Pandya, 2007).

We next examined the relationship between core ROIs and the five clusters previously identified from the functional connectivity matrices linking all 40 FPC-specific ROIs. This comparison revealed that core ROIs were found in four of the five clusters (Fig. 5 C). For each of these four clusters, connectivity from any FPC-specific ROIs to core ROIs within the same cluster (e.g., ROIs in cluster 1 to core ROIs in cluster 1) was significantly stronger than connectivity to within cluster peripheral ROIs ($p = 7.05 \times 10^{-11}$, $p = 5.56 \times 10^{-9}$, $p = 3.33 \times 10^{-9}$ and $p = 5.51 \times 10^{-12}$ for clusters 1–4 respectively, post-hoc t-tests, Bonferroni correction for multiple comparisons) or connectivity to core ROIs from other clusters ($p = 3.32 \times 10^{-12}$, $p = 1.21 \times 10^{-8}$, $p = 1.65 \times 10^{-7}$, and $p = 2.46 \times 10^{-5}$, for clusters 1–4 respectively, Fig. 5D). These data suggest that clusters 1–4 consist of a combination of “core ROIs” with direct anatomical connections to FPC, and a number of “peripheral ROIs” which aren’t directly connected to FPC but which are strongly connected to core ROIs from the same cluster. However, no core ROIs were found within cluster 4, which exclusively consisted of regions of

anterior temporal lobe. Further analysis of the connectivity of FPC-specific ROIs within cluster 4 revealed that these areas were weakly connected to core ROIs in the remaining clusters (Fig. S1). However, the strongest connection between ROIs in cluster 4 and core ROIs was to core ROIs in cluster 5 (consisting ventrolateral prefrontal cortex). The connection between ROIs within cluster 4 and core ROIs from cluster 5 was significantly stronger than to core ROIs from other clusters ($p = 6.19 \times 10^{-8}$) or to other peripheral ROIs within cluster 4 ($p = 0.04$, Fig. 5D).

2.5. Changes in network connectivity associated with lesion of FPC

Having identified a network of FPC-specific ROIs we next examined the changes in the relationship between those ROIs following lesion of FPC. Visualisation of the connections between the network of FPC-specific ROIs using multidimensional scaling (MDS) revealed that the lesion of FPC had a marked impact on the modular organisation of the network and a disruption of the previously described clusters (Fig. 6A.

ii). A repeated measures ANOVA (see Materials and Methods) calculated from the Euclidean distance between the centre points of the five clusters in FPC-control and lesion groups confirmed a significant main effect of lesion ($F_{(1,14)} = 18.88, p = 6.72 \times 10^{-4}$) and a significant interaction between lesion and cluster ($F_{(9126)} = 13.079, p = 1.43 \times 10^{-14}$).

Post-hoc t-tests on the estimated marginal mean distances between cluster centres (using Bonferroni correction for multiple comparisons, Fig. 6C.iii) revealed that lesion of FPC was associated with complex changes in the relationship between clusters 1–5. The most pronounced change was in the distance between clusters 1 and 3 which decreased significantly after lesion of FPC (Euclidean distance 5.87 ± 0.26 in FPC-control group vs. 3.60 ± 0.45 in FPC-lesion group, $p = 7.51 \times 10^{-4}$). In addition, the clear separation between cluster 2 and both cluster 4 (4.02 ± 0.19 vs. $2.36 \pm 0.34, p = 8.82 \times 10^{-5}$) and cluster 5 (6.21 ± 0.27 vs.

$2.56 \pm 0.47, p = 9.12 \times 10^{-6}$) was significantly decreased in the FPC-lesion group compared to the FPC-control. Secondary to these effects several additional changes in cluster separation were observed. The distance between cluster 1 and both clusters 4 (5.78 ± 0.28 vs. $4.07 \pm 0.49, p = 8.50 \times 10^{-3}$) and 5 (6.92 ± 0.29 vs. $5.00 \pm 0.51, p = 5.60 \times 10^{-3}$) decreased after lesion to FPC. In addition, the distance between clusters 2 and 3 (6.78 ± 0.20 vs. $4.84 \pm 0.35, p = 3.23 \times 10^{-4}$) and clusters 4 and 5 decreased after lesion of FPC (2.91 ± 0.21 vs. $1.92 \pm 0.37, p = 0.035$). While the distance between clusters 1 and 2 (3.46 ± 0.23 vs. $3.59 \pm 0.40, p = 0.79$) and between clusters 3 and 4 (4.71 ± 0.28 vs. $3.75 \pm 0.49, p = 0.11$) were not significantly different in the FPC-control and FPC-lesion groups; and the separation between clusters 3 and 5 significantly increased after lesion of FPC lesion (3.10 ± 0.17 vs. $4.86 \pm 0.29, p = 1.30 \times 10^{-4}$).

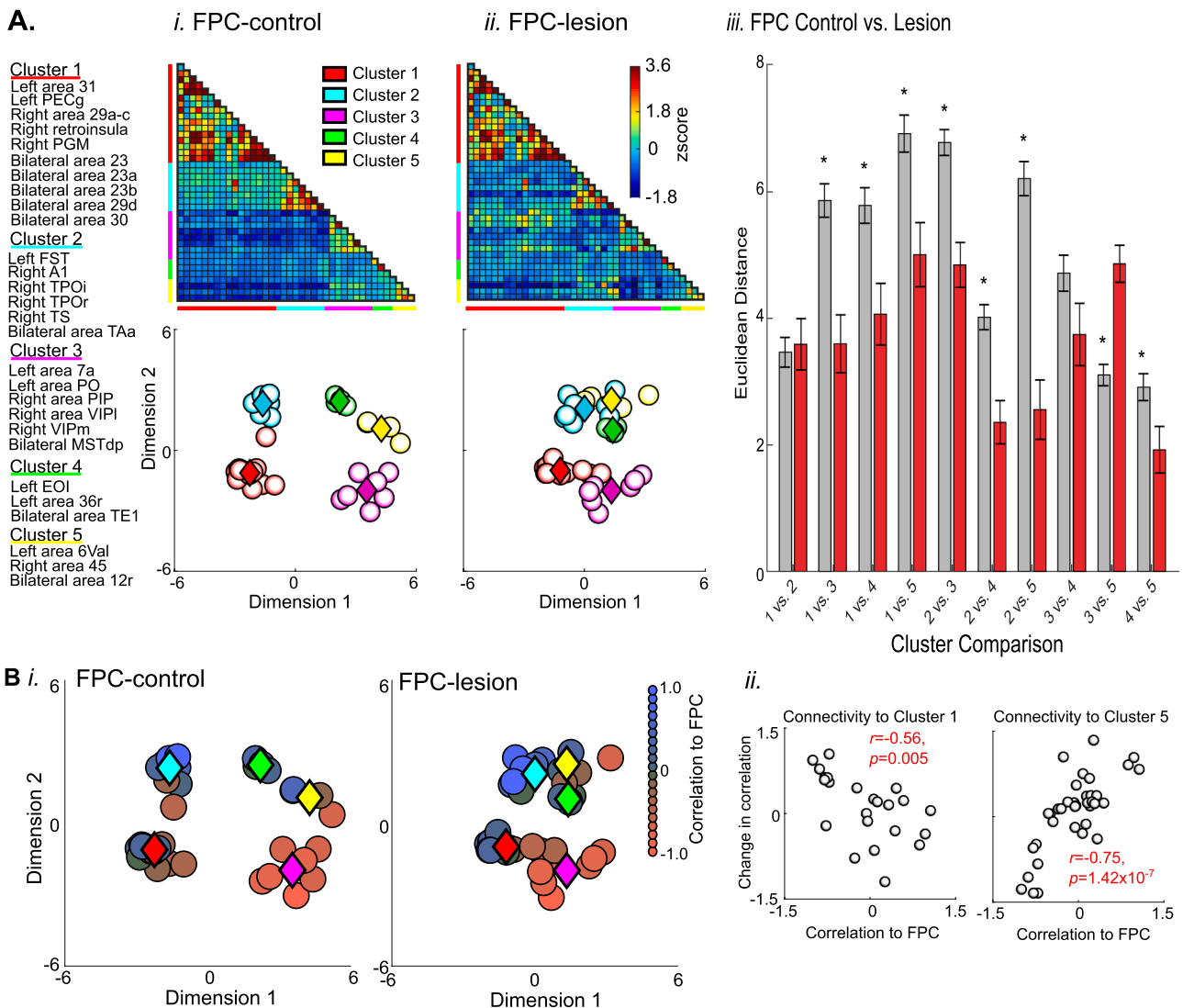


Fig. 6. The analysis of FPC-lesion specific changes in functional connectivity. **A.** Functional connectivity matrices and multidimensional scaling plots calculated from pair-wise correlations between the FPC-specific-ROIs in the FPC-control (Ci) and FPC-lesion groups (Cii). Within the connectivity matrices FPC-specific-ROIs are arranged by cluster (indicated by the colour bars to the bottom and left of the matrices), with a cluster-by-cluster breakdown of the FPC-specific-ROIs shown to the left of the connectivity matrices. Within the MDS plots, FPC-specific-ROIs are represented as circles coloured according to cluster class and are arranged such that the distance between ROIs corresponds to the similarity/dissimilarity between their patterns of connectivity. The centroid of each cluster, corresponding to the average connectivity of that cluster are depicted as coloured diamonds. Ciii. Bar chart showing the Euclidean distance between cluster centroids in the FPC-control (grey) and FPC-lesion groups (red). **B.** Correlation analysis showing the relationship between connectivity to FPC in control animals and lesion induced changes in connectivity. Bi. Multi-dimensional scaling plots showing 40 FPC-specific ROIs and 5 clusters in the FPC-control and FPC-lesion groups. ROIs coloured according to the control group strength of each ROIs connection to FPC or PS, respectively. Bii. Scatterplots showing significant correlations between the control group connectivity to FPC and the difference in control vs lesion group connectivity to cluster 1 (left panel) and the difference in control vs lesion group connectivity to cluster 5 (right panel). Non-significant correlations shown in Fig. S2. Note within cluster comparisons removed from all scatterplots.

Intriguingly, these data suggest that lesion of FPC caused two primary effects on connectivity between FPC-specific ROIs. Firstly, an increase in connectivity between ROIs in the posterior cingulate cortex and the parietal lobe. Secondly, an increase in connectivity between FPC-specific ROIs distributed throughout the temporal lobe and the ventral prefrontal cortex. To better understand the effect of FPC lesion we conducted a further analysis which explored whether changes in ROIs connectivity post-lesion was correlated with the strength of ROIs connection to the lesion site in control animals (Fig. 6). For the FPC-lesion, the change in connection strength (FPC-control vs. FPC-lesion) was calculated between each of the 40 FPC-specific-ROIs and each of the 5 clusters.

Correlation of this change in connection strength with the strength of each ROIs connection to FPC in control animals revealed two significant correlations (Figure 6Bi). Firstly, there was a significant negative correlation between the strength of an ROIs connection to FPC in control animals and the change in connection strength between those regions and cluster 1 after lesion of FPC (Figure 6Bi, Pearson's $r = -0.56$, $p = 5.0 \times 10^{-3}$). Secondly, there was a positive correlation between the strength of an ROIs connection to FPC in control animals and the change in connection strength between those regions and cluster 5 after lesion of FPC (Pearson's $r = 0.74$, $p = 1.01 \times 10^{-7}$). There was no significant correlation between the strength of ROIs connection to FPC in control animals and the change connection strength between those ROIs and either cluster 2, 3 or 4 after lesion of FPC (Pearson's $r = -0.23$, $r = -0.005$, $r = 0.31$, and $p = 0.21$, $p = 0.98$, $p = 0.063$, respectively. Non-significant correlations shown in Figure S2).

These data suggest two mechanistic insights into the effect of FPC-lesion on network connectivity. Firstly, FPC-specific-ROIs with strong, positive correlations to FPC in control animals became more closely connected to cluster 5 (consisting of frontal areas inc. 12r, 45, and 6Val) and weakly or negatively connected with cluster 1 (consisting primarily of posterior cingulate cortex area 23) after FPC lesion. Conversely, FPC-specific-ROIs with strong, negative correlations to FPC in control animals became more closely connected to cluster 5 and weakly or negatively connected with the frontal regions consisting of cluster 1 (Figure 6Ai).

Finally, we conducted two control analyses to confirm that both the selected network of FPC-specific ROIs, and the changes in connectivity within this network following lesion of FPC were specific to that lesion. The first control analysis repeated the whole brain search analysis described previously using the second PS-lesion SVD component. This analysis identified only 15 PS-specific-ROIs with difference fingerprints that fit the pattern of the second PS-lesion SVD component significantly better than expected by chance (one sided permutation test, $p < 0.05$, corrected for multiple comparisons using FDR). Therefore, to provide a meaningful comparison with the previous FPC-lesion analysis (i.e. 40 regions), we applied a relaxed criterion ($p < 0.1$, corrected for multiple comparisons using FDR) that revealed 42 PS-specific-ROIs in the PS-control group.

The analysis revealed little overlap between the FPC and PS-specific ROIs. In contrast to the FPC-specific ROIs which included the majority of posterior cingulate subdivisions, the only comparable PS-specific ROI was small area of dorsal posterior cingulate (area 31). PS-specific ROIs were identified throughout posterior parietal cortex, including several areas anterior to the postcentral gyrus and sulcus (including areas 7op in the left hemisphere and bilaterally areas 7t, AIP, LIPv) as well as a number of regions distributed along the parietal-occipital boundary (including LOP, V4tp and MSTm bilateral). However, most of these ROIs were included in the FPC-specific network, the only overlap between the FPC and PS specific ROIs in the posterior parietal cortex was MSTdp and VIPI. In the temporal lobe PS-specific ROIs included left IPa, the temporal pole (left TPPai and bilateral TPPpro), as well as right PaS (parahippocampus) and bilateral STS area 1. But no PS-specific regions overlapped with FPC-specific ROIs previously described. In the frontal lobe two areas of premotor cortex were included in the PS-specific ROIs

(left area 6M and right area 6DR). More anteriorly a large number of prefrontal regions were included as the PS-specific ROIs. Area 12r was consistently included as an affected by both lesion of both PS and FPC. However, area 12l, 13a, 13b, 13l, 14r and 24b were also included as PS-specific ROIs (Fig. 7B).

Secondly, we conducted a further analysis which examined the effect of a PS lesion on connectivity between the FPC-specific-ROIs (Fig. 7 C). This repeated measures ANOVA examining the Euclidean distance in PS-control and PS-lesion groups between the centres of all 5 clusters identified as specific to the FPC-lesion did not reveal a significant effect of lesion ($F_{(1,14)} = 0.49$, $p = 0.50$) or an interaction between lesion and cluster ($F_{(9126)} = 1.00$, $p = 0.44$, Fig. 7 C).

3. Discussion

Here we show that circumscribed bilateral lesions to macaque FPC cause distinctive changes in rsfc across a network of brain regions distributed across the parietal and temporal lobes as well as within the prefrontal cortex. This network consisted of 'core ROIs,' principally distributed between ventrolateral prefrontal cortex (including areas 12r and 45), posterior cingulate cortex (including areas 23, and 30), and superior temporal gyrus (including areas TAA, TPOR and A1). Core ROIs possessed strong anatomical connections to FPC, were consistently found to have a substantial number of strong functional connections to other FPC-specific ROIs and appeared to determine the modular structure of the network. By contrast 'peripheral ROIs' lacked connections to FPC but were in turn functionally connected to this core network. Crucially we were able to isolate this network of FPC-specific ROIs from more generalised effects of prefrontal damage by contrasting the changes in connectivity observed following lesion of FPC with those of PS. Within this FPC-specific network the lesion induced a marked change in network structure of FPC-specific ROIs that may be summarised according to two significant trends: (i) ROIs with weak connections to FPC become more strongly correlated to posterior cingulate cortex; (ii) whilst those with strong functional connections to FPC become more strongly connected to ventrolateral prefrontal cortex.

These findings emphasize the importance of a network of functional connections between FPC and two primary sites, posterior cingulate cortex and ventrolateral prefrontal cortex. We propose that these regions may constitute a sub-network that may also be co-activated during behaviour to facilitate rapid learning and evaluation between behavioural alternatives. Here we first discuss the anatomical and functional basis for our selection of FPC-specific ROIs, as well as the importance of dissociating the specific effects of FPC-lesions from those associated with lesions of PS. Then we consider the previously published behavioural deficits caused by FPC lesions in light of the changes in connectivity described here and discuss the potential implications for our findings with respect to current theories of FPC function.

3.1. Constituent regions of the FPC-specific network

By focusing on lesion-induced differences in rsfc, the current study has defined a network upon which FPC has a direct causal influence. The FPC-specific network included regions of cortex distributed both within prefrontal cortex (predominately ventrolateral prefrontal cortex) and extending more posteriorly to regions of the superior temporal sulcus and gyrus, parietal lobe, posterior cingulate cortex, and temporal pole. Within this network ROIs were connected in a complex fashion, with five functionally distinct clusters evident in the connectivity matrix: (i) a posterior cingulate and medial parietal cortex cluster (cluster 1); (ii) a superior and middle temporal cortex (cluster 2); (iii) a posterior parietal and medial superior temporal cortex (MST) cluster (cluster 3); (iv) a temporal polar cortex cluster (cluster 4); and (v) a ventrolateral prefrontal cortex cluster (cluster 5).

We propose that our network of FPC-specific ROIs consists of two sub-divisions, namely 'core' and 'peripheral' ROIs. Core ROIs, defined

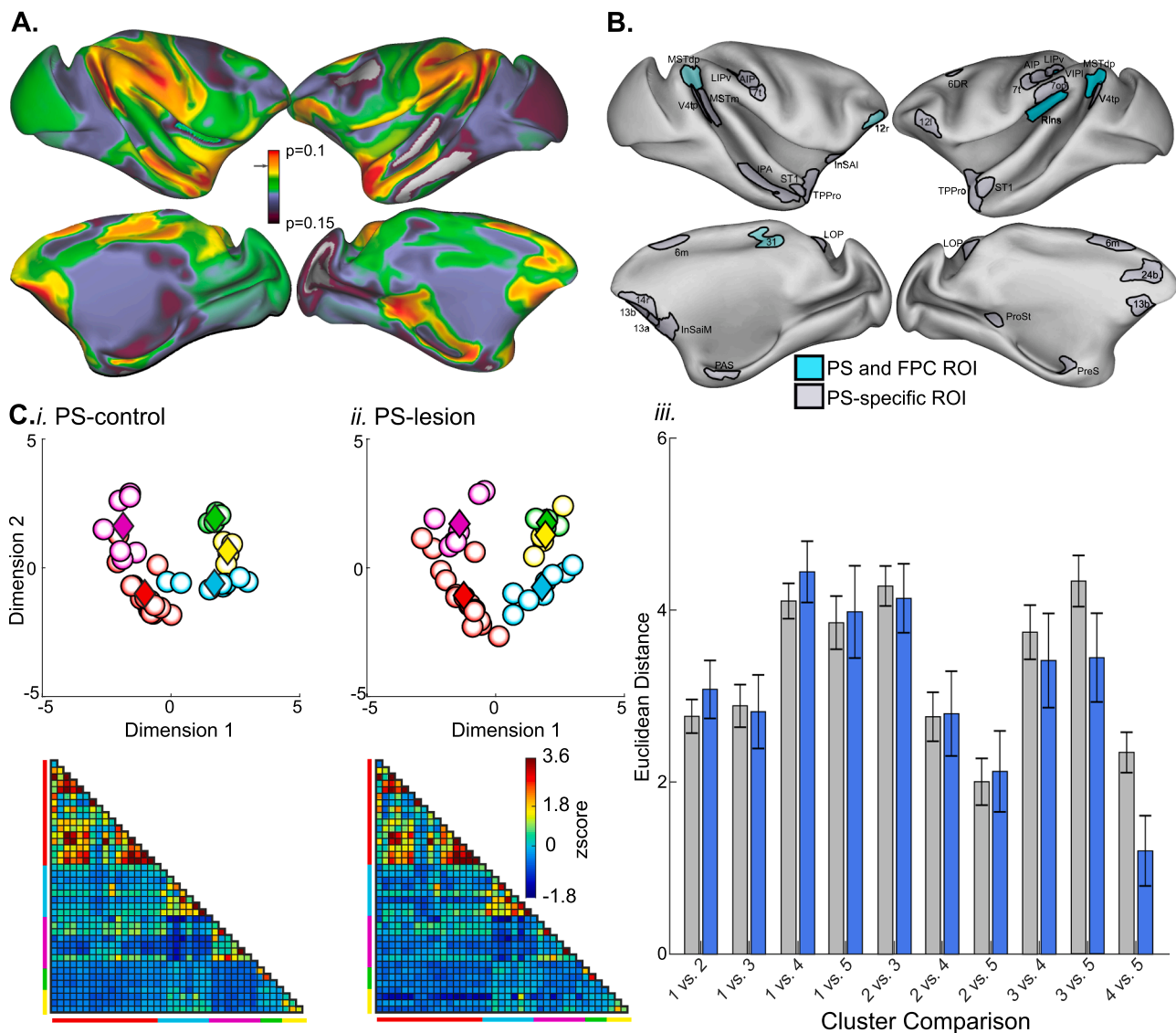


Fig. 7. Confirmation of the dissociation between the network of FPC-specific ROIs and the effects of PS lesion. **A.** Surface maps showing the results of a whole brain search for cortical regions with PS-lesion induced changes in functional connectivity matching the second PS-SVD component. A total of 40 PS-specific-ROIs were identified in which changes in connectivity matched this SVD component better than expected by chance ($p < 0.1$ permutation test corrected for multiple comparisons with FDR, see Materials and Methods for full details of the whole brain search). Gray arrow on the colourbar indicates $p = 0.1$. **B.** Surface maps showing overlap between FPC-specific ROIs and PS-specific ROIs. ROIs included in both networks shown in cyan, non-overlapping ROIs shown in grey. **C.** Analysis confirming that lesion of PS did not affect connectivity between FPC-specific ROIs. Functional connectivity matrices and multidimensional scaling plots calculated from pair-wise correlations between the FPC-specific-ROIs in the PS-control (Ci) and PS-lesion groups (Cii). Within the connectivity matrices FPC-specific-ROIs are arranged by cluster (indicated by the colour bars to the bottom and left of the matrices). Clusters and labels are consistent with those in Fig. 6. Within the MDS plots, FS-specific-ROIs are represented as circles coloured according to cluster class and are arranged such that the distance between ROIs corresponds to the similarity/dissimilarity between their patterns of connectivity. The centroid of each cluster, corresponding to the average connectivity of that cluster are depicted as coloured diamonds. Ciii. Bar chart showing the Euclidean distance between cluster centroids in the PS-control (grey) and PS-lesion groups (red).

on the basis of the strength of their functional connections to other ROIs within the network, were found predominantly in three locations: ventrolateral prefrontal cortex, posterior cingulate cortex, and the superior temporal sulcus and gyrus. All core ROIs had moderate to strong anatomical connections to FPC, and two of these sites, posterior cingulate and superior temporal cortex have direct white matter connections to FPC, via the extreme capsule and cingulum bundle respectively (Petrides and Pandya, 2007). By contrast, peripheral ROIs were well connected to core ROIs, but in comparison to core ROIs, had predominantly weak or moderate anatomical connections to FPC. Core ROIs were found within four of the five clusters described above, and connectivity between these ROIs and other within cluster core ROIs was significantly higher than connectivity to core ROIs in other clusters or to

non-core ROIs. We therefore propose that the FPC-specific network consists principally of core ROIs at three sites (vIPFC, PCC and STG), as well as associated peripheral ROIs with strong functional connections to these core regions. It is important to note that the network we present here is based solely on the FPC-specific component derived from our analyses. Whilst our SVD analysis did identify further changes in connectivity associated with lesion of FPC, such changes were also observed after lesion of PS. Therefore further research is needed before we can conclude whether these shared ROIs participate in meaningful resting state networks with FPC, or indeed whether there are changes in connectivity which can be readily observed following a damage to a variety of prefrontal cortical regions.

Although the core ROIs within our network all show moderate or

strong anatomical connections to FPC, the strength of functional connections between these ROIs and FPC was inconsistent, and a number of core ROIs had weakly positive or even negative correlations to FPC. This dissociation between structural and functional connection strength is particularly notable as several studies have explored the relationship between these two types of connectivity in the brain. Examples where anatomical tracing has been paired with the estimation of functional connectivity between ROIs have revealed both considerable overlap between the extent of functional and anatomical connectivity to a seed (Vincent et al., 2007), and also consistency in the strength of anatomical and functional connectivity between pairs of ROIs (Vezoli et al., 2021).

However, the relationship between strength of structural and functional connections between two regions is complex, with functional connectivity modified by various additional factors. For example, strength of functional connections between two areas is influenced both by the distance between them (Ercsey-Ravasz et al., 2013; Vezoli et al., 2021) and by indirect, polysynaptic connections (Honey et al., 2009; Vincent et al., 2007). Furthermore, cortical networks defined by strength of functional connectivity frequently include regions without direct anatomical connections (Hutchison et al., 2010; Vincent et al., 2007).

Our network of FPC-specific ROIs supports both sets of observations. The strong positive correlation between the strength of functional and anatomical connections between FPC-specific ROIs and FPC resembles the correlation between anatomical and functional connectivity demonstrated previously across the entire brain (Honey et al., 2007). Whilst observations of weak functional connectivity for many core ROIs with known anatomical connections to FPC (e.g., area 23 and 30), and conversely of strong functional connections between peripheral ROIs and FPC without strong anatomical connections (e.g., FST, 7a and PIP), likely reflects the impact of distance from FPC to core ROIs, and polysynaptic communication to FPC respectively.

3.2. Dissociating an FPC-specific network

Regions of prefrontal cortex are robustly connected to neighbouring areas and are therefore highly correlated at rest (Hutchison et al., 2011). FPC and PS are no exception, sharing direct connections with a number of prefrontal regions especially within vlPFC, and orbitofrontal cortical areas (Markov et al., 2014; Petrides and Pandya, 2007; Saleem et al., 2014). Whilst overlap between regions with direct anatomical connections to FPC and PS is less pronounced outside the prefrontal cortex there are notable exceptions, likely due to commonly shared white matter tracts (see Materials and Methods for a detailed commentary on differential effects on white matter tracts of the two lesions). Both FPC (area 10) and the dorsal bank of the PS (area 46d) are well connected to superior temporal gyrus, sulcus and adjacent insula cortex (Markov et al., 2014; Saleem et al., 2014), via branches of the extreme capsule (Schmahmann and Pandya, 2006). With both FPC and to a less extent PS well connected to regions of posterior cingulate cortex (Markov et al., 2014; Saleem et al., 2014). It is therefore unsurprising that the first pass whole-brain analysis of regions affected by FPC and PS lesions revealed considerable overlap with 27% of affected ROIs common to both lesions. The majority of these shared ROIs were located in the parietal (e.g., area 7, PIP and VIP) and frontal lobes (e.g., insular cortex and premotor cortex). Notably, several of these ROIs are thought to be weakly connected to FPC (e.g., area 7 and area 6, as well as somatosensory cortex and visual areas V3 (Markov et al., 2014; Petrides and Pandya, 2007)). That these regions are affected by these lesions of FPC further emphasises the findings of previous studies, that functional connectivity does not necessarily reflect underlying anatomical connectivity (Hutchison et al., 2011; Vincent et al., 2007). Understanding both the similarities and differences between anatomical and functional connections will be important for advancing understanding of the contributions brain regions make to cognition.

Given this shared connectivity associated with FPC and PS we

utilised a whole brain search for specific connectivity fingerprints. In contrast to previous studies, in which the connectivity fingerprints were defined to find regions with homologous patterns of connectivity or across species (Neubert et al., 2014; Saleem et al., 2014), here we created FPC and PS specific fingerprints based on the first two components of a singular value decomposition (SVD) of connectivity between all ROIs. Decomposition of connectivity matrices in this fashion enabled us to identify pattern of changes specific to both lesions, and therefore to identify a network of ROIs affected by both lesions. Importantly the whole-brain search to identify FPC-specific ROIs was assumption free and regions could potentially be identified as both FPC and PS specific. Therefore our subsequent analysis included steps to validate our approach. Firstly, the networks of FPC-specific and PS-specific ROIs isolated by this technique had very little overlap. Secondly, connectivity between the specific networks of ROIs associated with FPC and PS were unaffected by lesion of the alternative region (be it FPC or PS). It may therefore be that the combination of data compression techniques with whole-brain fingerprint searches provides additional power to better explore whole-brain functional connectivity, particularly in understanding connectivity of regions of prefrontal cortex, where extensive anatomical interconnectivity has been clearly demonstrated.

One further complication in separating the changes in connectivity associated with FPC from PS is the extent of direct but inadvertent damage caused to underlying white matter tracts during neurosurgery. Previous research has demonstrated that inadvertent white matter tract damage after bilateral aspiration lesions to orbitofrontal cortex (OFC) should be taken into account when attributing causal effects to aspiration lesions (Rudebeck et al., 2013). However, while important for OFC, the situation is quite different when considering FPC aspiration lesions simply because FPC lesions are largely without such confounds. Unlike the case for OFC, the white matter underneath FPC cortex primarily contains fibres that originate or terminate in FPC per se. Hence any white matter tracts inadvertently disrupted by the lesion are one and the same as those we expect to be mediating the influences FPC cortex has on widespread cortical regions our data speaks to. In our detailed commentary in the [Supplementary Materials](#), we compare the routes and locations of relevant prefrontal white matter fibres, and the extent to which white matter tracts are differentially disrupted by the FPC versus PS lesions. We have previously discussed, in similar detail, which fibre tracts may be damaged after aspiration lesions to more superior dorsolateral prefrontal cortex aspiration lesions than our mid-dorsolateral prefrontal (PS) lesion here which despite some overlap are distinctly different (Kwok et al., 2019).

Finally, it is important to note that the PS lesions in this study were only unilateral, and that right PS was intact in both animals. Bilateral PS lesions should clearly be regarded the ideal control to isolate FPC-specific changes in connectivity. However, several observations from control analysis suggest that the changes in connectivity associated with unilateral lesions of PS are sufficient to dissociate any changes common to lesions of both PS and FPC from those specific to FPC alone.

Firstly, bilateral changes in functional connectivity are not uncommon after unilateral cortical lesion or damage, perhaps arising because of interhemispheric connections between homologous cortical areas (Vincent et al., 2007), and have been reported in both humans (Voytek et al., 2010) and macaques (Adam et al., 2020; Ainsworth et al., 2018). A control analysis, which compared ipsilesional with contralesional changes in connectivity confirmed these studies, demonstrating that comparable changes in connectivity occurred between prefrontal, temporal and parietal ROIs in both hemispheres after lesion of left PS (Figure S3).

Furthermore, comparison of the regions which were affected by unilateral lesion of PS and those affected after both left and right PS had been lesioned (albeit serially rather than simultaneously), revealed a high degree of overlap between areas. Particularly in regions located within the frontal and parietal lobes such as premotor (e.g., area 6Vb, and 6Vam) and somatosensory cortex (e.g., areas 2 and 3). Most

importantly, the 2nd SVD components calculated from the FPC-lesion fingerprints, was uncorrelated with the corresponding 2nd SVD component calculated from changes in connectivity caused by lesion of left and then right PS. Therefore, whilst the unilateral nature of the PS lesion limits our ability to draw firm conclusions regarding a network of regions affected by a bilateral lesion of PS, the data still provide a meaningful contrast to the FPC lesion studied here. In addition, the FPC and PS lesion datasets (all of which are available via https://github.com/mainworthpsy/FPC_Lesion) provide important resources for researchers to isolate further networks of ROIs they are interested in that are affected specifically by bilateral lesions of FPC or unilateral lesions of PS.

3.3. The relationship between behavioural deficits, and changes in connectivity within the FPC-specific following lesion of FPC

Lesions of FPC caused marked changes in connectivity within the network of FPC-specific ROIs. Following the lesion, separation between posterior cingulate and posterior-parietal cortex (clusters 1 to cluster 3), and between ventrolateral prefrontal/premotor cortex and both superior temporal cortex and temporal polar cortex (cluster 5 to clusters 2 and 4) decreased. These changes in connection strength between FPC-specific ROIs and ROIs within clusters 1 and 5 were significantly correlated with the strength of an ROIs connection to FPC (Fig. 6B), implying that FPC has a crucial role in influencing connections from posterior cingulate cortex and ventrolateral prefrontal cortex.

The three FPC-lesion animals used in this study received equivalent behavioural testing pre and post lesion. Post-lesion these animals demonstrated specific behavioural impairments, namely deficits in rapid learning about the relative value of alternatives from single trials in memory paradigms and also deficits in rapid learning of new alternative abstract rules (Boschin et al., 2015). However, they performed at a level comparable to control animals when required to perform a range of other tasks including working memory tasks, namely delayed matching-to-sample, delayed nonmatching-to-sample, and reversals between these tasks (for a full account of the behavioural deficits see Boschin et al., 2015; for a review of the behavioural differences of FPC and PS lesion see Boschin and Buckley, 2015; and for details of additional effects of FPC lesions on other abstract rule tasks see Buckley et al., 2009; Mansouri et al., 2015; Mansouri et al., 2019). The extent to which the behavioural deficits described above can be ascribed to disruption across a wider network of cortical areas connected to FPC is currently unknown. Given the changes in functional connectivity between FPC, posterior cingulate, and ventrolateral prefrontal cortices, which followed lesion of FPC, it is tempting to conclude that these deficits are directly related to disrupted communication between these areas. However, it is important to stress that for now this is purely a correlative association, and further work is needed to explore the relationship between the aforementioned behaviours and specific pathways, or combinations of pathways, linking FPC, with the rest of the brain.

Notably, recent studies have proposed methods capable of linking both the strength of connectivity (Finn et al., 2015) or directed information flow (Chén et al., 2019) within cortical networks to behavioural performance. However, these measures typically require both behavioural testing and resting state data from large cohorts of subjects, far in excess of what has been possible for combined imaging/lesion studies utilising NHPs (Adam et al., 2020; Ainsworth et al., 2018; O'Reilly et al., 2013; Pelekanos et al., 2020). Given this limitation it seems likely that future research in NHPs into the nature of connectivity between these regions will instead focus on quantifying the nature of inter-area interactions whilst animals perform cognitive tasks (Dal Monte et al., 2020).

To conclude, our study has emphasised the importance of FPC to a network of 'core ROIs' located in ventrolateral prefrontal cortex, posterior cingulate cortex, and superior temporal gyrus. The primary effect of a lesion to FPC is to disturb functional connectivity of posterior

cingulate and ventrolateral prefrontal cortex. We therefore suggest that FPC, posterior cingulate and ventrolateral prefrontal cortex comprise a network of cortical areas specialised for learning relative values of alternatives based on highly processed abstract information. Future work should investigate communication between these three areas of cortex, with the aim of linking dynamic changes in network connectivity with ongoing behaviour. As causal evidence will be crucial, such study may involve traditional interventions such as crossed-disconnection surgical approaches, muscimol infusion, or electrical micro-stimulation through implanted multi-electrode arrays, or more recently developed reversible intervention methodologies including pathway specific optogenetic and chemogenetic manipulation (e.g. Designer Receptors Exclusively Activated by Designer Drugs, DREADDS) or focussed ultrasound neuromodulation. Regardless of the technique utilised the combination of an interventional technique with behavioural and neural recordings (e.g. multi-area electrophysiology, fMRI) will be essential for future efforts to assess causal influences that local brain regions exert upon a wider network at the neuronal level, that together underlie cognition.

4. Materials and methods

4.1. Animals

Resting state fMRI and structural scans were collected under anaesthesia from a total of thirty macaque monkeys (*Macaca mulatta*), divided between two experimental branches and four experimental groups.

The first branch, consisting of sixteen monkeys, assessed the impact of FPC lesions on whole brain functional connectivity. Within this branch, one experimental group received bilateral lesions of FPC (area 10, Fig. 1B) and were scanned circa 8 weeks post-operatively. This FPC-lesion group comprised three female monkeys with an average age and weight of 7.6 (7.3–7.8) years and 7.8 (7.0–9.4) kg at time of scanning. Within this branch we also collected resting-state fMRI data in a directly comparable unoperated FPC-control group of thirteen monkeys. This FPC-control group comprised one female and twelve male monkeys, with an average age and weight of 4.5 (3.6–7.5) years and 7.6 (6.3–12.8) kg at time of scanning. The groups were directly comparable because all MRI data from both groups under this experimental branch was collected under sevoflurane anaesthesia.

The second branch, consisting of fourteen monkeys, were used to assess the impact of PS lesions on whole brain connectivity. Within this branch one experimental group received unilateral lesions of both banks of the left PS (including area 46 and 9/46, Fig. 1C) and were scanned circa. 6 weeks post-operatively. This PS-lesion group comprised two male monkeys with an average age and weight of 6.4 (6–6.75) years and 9.5 (8.8–10.4) kg at time of scanning. As reported elsewhere, each PS-lesion animal had two post-lesion scanning sessions, and therefore scanning session was used as the experimental observation for this group (Ainsworth et al., 2018). Within this branch, we also collected resting-state fMRI data in a directly comparable PS-control group of twelve monkeys. This unoperated PS-control group comprised twelve males, with an average age and weight of 4.0 (3.3–5.5) years and 7.1 (5.7–12.6) kg at time of scanning, several PS-control animals have been collated as part of the PRIME-DE consortium (Milham et al., 2018). All MRI data from both groups in this second experimental branch was collected under isoflurane anaesthesia.

All animals were socially housed in enriched environments with a 12 hr light/dark cycle and had ad libitum water access. Prior to participation in this study, all lesioned animals from both branches received basic training on an identical set of behavioural tasks reported elsewhere (Ainsworth et al., 2018; Boschin et al., 2015). All animal surgery, anaesthesia, and experimental procedures were carried out in accordance with the guidelines of the UK Animals (Scientific Procedures) Act of 1986, licensed by the UK Home Office, and approved by Oxford's Committee on Animal Care and Ethical Review.

4.2. Surgery

Bilateral lesions of FPC (macaque area 10) were carried out by aspiration of cortical tissue under sterile conditions. The caudal limit of the lesion on the dorsolateral surface was 2 mm posterior to the rostral tip of the principal sulcus. On the orbital and medial cortical surfaces, the lesion extended caudally to match the same anterior-posterior extent of the lesion on the dorsolateral surface. See [Boschin et al. \(2015\)](#) for further details of surgical procedures. Unilateral lesion of both banks of left PS (area 46 and 9/46) was performed by aspiration of cortical tissue under sterile conditions. The unilateral lesion covered left dorsal and ventral banks of PS. For further details of surgical procedures see [Ainsworth et al. \(2018\)](#). In removing grey-matter care was taken to preserve sub-cortical white-matter, where possible. Drawings of brain lesion locations in the FPC- and PS-lesion animals are presented in [Fig. 1](#).

4.3. Anaesthesia and MRI data acquisition

Anaesthesia was induced with intramuscular injection of ketamine (10 mg/kg), xylazine (0.125–0.25 mg/kg) and midazolam (0.1 mg/kg) two hours prior to the start of scanning, which allowed ketamine to leave in the monkey's bodies before data acquisition. After induction, anaesthesia was maintained using sevoflurane for FPC-lesion and FPC-control animals and isoflurane for PS-lesion and PS-control animals. Commonly used volatile anaesthetics including sevoflurane (i.e. above 2.0%) and isoflurane (i.e. above 1.5%) have been shown to modulate functional connectivity in the brain in a dose dependent manner ([Hutchison et al., 2014](#); [Peltier et al., 2005](#)). Therefore, to preserve connectivity and minimize variation in the data EPI data was collected during light anaesthesia, with a targeted sevoflurane concentration of 2.0% and a targeted isoflurane concentration of 1.5% across the entire project. There was no significant difference between the sevoflurane concentrations from animals in the FPC-control and FPC-lesion group (average concentrations of sevoflurane, 2.1% and 2.4% respectively, $t_{(14)} = -1.145$, $p = 0.271$, two-tailed) and no significant difference between the isoflurane concentrations from animals in the PS-control and PS-lesion group (average concentrations of isoflurane, 2.0% and 1.7% respectively, $t_{(14)} = 0.69$, $p = 0.50$, two-tailed t-test). Physiological parameters (e.g. heart rate and blood pressure) were used to assess the depth of anaesthesia throughout the scanning sessions (For further details of anaesthesia maintenance and monitoring see [Mars et al., 2011](#); [Mitchell et al., 2016](#)).

fMRI data was collected using a horizontal 3 T scanner using a custom-made 4-channel phased array coil (H. Kolster, MRI Coil Laboratory, Laboratory voor Neuron Psychofysiologie, KU Leuven). During scanning animals were placed in an MRI compatible stereotaxic frame to ensure head stabilisation. High-resolution structural scans (0.5 mm isotropic voxels) were acquired using a T1-weighted high-resolution magnetization-prepared rapid-acquisition gradient echo (MPRAGE) sequence (128 slices, TR=2500 ms; TE=4.01 ms). Whole-brain resting-state EPI fMRI data were collected at a 2x2x2mm resolution (36 axial slices, TR=2000 s, TE=19 ms), with an approximate duration of 54 min for each animal (1600 volumes). As two differing anaesthesia regimes were utilised for the FPC and PS lesions we carried out no direct comparisons of the changes in connectivity associated with both lesions. Furthermore, we carried out a control analysis in control animals within the FPC-specific ROIs which showed no significant difference between the two anaesthesia regimes ([Figure S4](#)).

4.4. MRI data pre-processing and calculation of functional connectivity

All fMRI data pre-processing and analysis was conducted using a combination of MATLAB (The MathWorks Inc.), SPM8 (Statistical Parametric Mapping; www.fil.ion.ucl.ac.uk/spm/), FSL (fMRI of the Brain (FMRIB) Software Library; <http://fsl.fmrib.ox.ac.uk/fsl/fslwiki/>), Caret (Computerized Anatomical Reconstruction Toolkit ([Essen, 2012](#)))

and aa software (automatic analysis ([Cusack et al., 2015](#)); www.automaticanalysis.org). High resolution structural images for each animal were aligned to a standard space (F99 Rhesus macaque template - in the space of the atlas of ([Saleem and Logothetis, 2012](#)) using affine and nonlinear transformations). Images were subsequently segmented into grey matter, white matter and cerebrospinal fluid (CSF) masks ([McLaren et al., 2009](#)). Resting-state fMRI data were aligned to standard space through a two-stage process and then spatially-smoothed with a 3 mm Gaussian kernel (full-width half maximum). Grey-matter masks were defined on a monkey-by-monkey basis as voxels with grey-matter probability > 0.5 within each animal.

Physiological noise covariates were calculated by extracting up to 6 principal components (sufficient to explain 99% of the variance) from the BOLD time-series for white-matter and CSF tissue masks ([Behzadi Y et al., 2007](#)). An additional vascular covariate was defined as the mean time-course within a mask encompassing the superior sagittal sinus. A motion covariate was calculated from the EPI data (prior to smoothing and registration) and was defined as the time-course of the average displacement over the expected brain volume. These confound time-series and their first derivatives were then regressed from each grey-matter time-series, and the mean time-series was calculated for each cortical region within the derived from the CC atlas (the LV-FOA-PHT composite atlas) for macaques ([van Essen et al., 2012](#)). Finally, functional connectivity was estimated by calculating pairwise correlation coefficients (Pearson's r) for each pair of CC areas (260 areas, 130 in each hemisphere) and then transformed using Fisher's r -to- z transform. For further details of the pre-processing of structural images & resting state data, see ([Ainsworth et al., 2018](#); [Mitchell et al., 2016](#)).

4.5. Nonparametric functional connectivity analysis

To identify functional connectivity between areas which changed significantly following lesions to FPC or PS, we carried out two separate, assumption-free, nonparametric permutation-tests ([Nichols and Holmes, 2001](#)) on the mean observed difference between the FPC-control and FPC-lesion groups, and the mean observed difference between the PS-control and PS-lesion groups, respectively. Note that prior to permutation test, bilateral areas 10o and 10 m were excluded from the 260 regions of the CC atlas in FPC-control and FPC-lesion groups and areas 46 v and 46p were excluded in PS-control and PS-lesion groups, resulting in the mean inter-area correlation matrices between 256 regions in both FPC groups (shown in [Fig. 2 A.i](#)) and both PS groups (shown in [Fig. 2 B.i](#)). For each lesion group versus its control group comparison, the test involved a comparison of the observed difference against a reference distribution of differences, under the null hypothesis of no significant change in the functional connectivity between the two groups. For each connection, the reference distribution was obtained by performing 10,000 permutations on the animal labels to randomly assign them to two groups; then accordingly, on each loop of the permutation the mean functional connectivity of that connection (for each of the two randomly constituted/permutated 'groups') was calculated and only the minimal and maximal difference was stored. This resulted in both a minimal and maximal matrix: each 256 by 256 (i.e. excluding area 10 m and area 10o bilaterally from 260 aforementioned cortical regions), when comparing FPC-control and FPC-lesion animals; and each 256 by 256 (i.e. excluding area 46p and area 46 v bilaterally from 260 cortical regions) when comparing PS-control and PS-lesion animals. The upper and lower thresholds were defined as the 97.5th percentile of the maximal matrix and the 2.5th percentile of the minimal matrix, respectively. Any observed mean difference between the FPC-lesion and FPC-control groups, or between the PS-lesion and PS-control groups, greater than the upper threshold or smaller than the lower threshold was deemed significant at the 0.05 level ($p < 0.05$, two-tailed). By selecting the maximal/minimal value from the permutation distribution, this two-sided nonparametric permutation-based test was sensitive to both

positive and negative changes in connectivity and therefore controlled for global type I errors associated with multiple comparisons. From these two non-parametric tests two lists of ROIs were identified, those ROIs identified as partaking in functional interactions affected by lesion of FPC and those affected by lesion of PS.

4.6. Connectivity fingerprint analysis

To better visualise the changes in functional connectivity which occurred following lesion of FPC and PS the connectivity of all 85 ROIs (identified as a result from the aforementioned non-parametric analyses) was visualised using connectivity fingerprints (Neubert et al., 2015, 2014; Passingham et al., 2002). We used polar plots to view the connectivity between each of these ROIs and a subset of 31 ROIs which occurred bilaterally (see Fig. 3). Each “spoke” in the fingerprint corresponded to one of the 31 bilateral ROIs and the functional connectivity fingerprints of all 85 ROIs were plotted as a separate line with radial distance from the centre corresponding to strength of the functional connection. To highlight similarities and differences, polar plots were constructed in this way for all four groups (i.e., FPC-control, FPC-lesion, PS-control, and PS-lesion). In addition, we calculated difference fingerprints for each ROI that visualised the difference between the lesion vs control comparison group averages; in these difference fingerprints the difference between the relevant control and post-lesion group (i.e., FPC-control vs. FPC-lesion, and PS-control vs. PS-lesion, respectively) are shown radially with zero indicating no difference between the two groups.

4.7. Singular value decomposition

To isolate changes in connectivity associated with the lesions of FPC or PS, we carried out singular value decomposition (SVD) of the large set of difference fingerprints for each lesion (i.e., large matrices composed of each of the bilaterally significantly involved ROIs ($n = 31$, see results) on one axis, showing its interaction with each ROI in the set of identified ROIs ($n = 85$, see results) on the other axis. This analysis reduced the 85 difference fingerprints into a series of orthogonal components. Within this series the first component explained the greatest proportion of variance of the matrix and therefore represented the primary change in connectivity associated with each lesion (contained within the right singular vector matrix), with subsequent components explaining the greatest proportion of the remaining variance of the matrix (and therefore the next most common pattern of changes in connectivity). Crucially, these components were calculated independently for each lesion and therefore covariance between FPC and PS components reflected changes in connectivity common to both lesions. The independence (or otherwise) of these components was tested by Pearson correlation of the corresponding components obtained from the FPC and PS difference fingerprints. Here we considered the first two components calculated from the two difference matrices for two reasons. Firstly, the two components together explained over 80% of the total variance associated with each lesion (given by the singular value matrix). Furthermore, there was no correlation between the second SVD components obtained from both FPC and PS difference fingerprint matrices, therefore the second FPC component represented the primary FPC specific change in connectivity.

We conducted a further whole brain analysis to determine for every brain region the extent to which their changes in connectivity associated with lesion of FPC and PS matched their relevant second SVD component. Difference fingerprints were calculated for each of the 256 atlas regions and multiplied by the right singular vector matrix to generate a loading score. To ensure statistical independence of this metric, the SVD analysis was recalculated in a leave one out fashion for each cortical area. To provide statistical inference, these scores were compared to those generated by repeating the procedure using a surrogate difference fingerprint matrix calculated by random permutation of the FPC-control

and FPC-lesion groups 10,000 times and random permutation of the PS-control and PS-lesion groups 10,000 times, separately. Significance was determined from root mean squared scores of both the random and real scores with sigma set at $p = 0.05$ in FPC groups and $p = 0.1$ in PS groups, correction for multiple comparisons was achieved by false detection rate (FDR).

4.8. Multi-dimensional scaling analysis

We visualised connectivity between the ROIs ($n = 40$ in FPC groups, see results) identified using SVD, both in the FPC-control and FPC-lesion groups using multi-dimensional scaling (MDS). To examine the relationship between these ROIs in the FPC-control group, a dissimilarity matrix was calculated from the group average connectivity matrix. Classical MDS was then carried out to generate an x and y position for each ROI in 2D space. Clustering of ROIs based on these 2D coordinates was then calculated by K-means clustering. The number of clusters for each group was found using the elbow method, explaining 95% of total variance.

Visualisation of connectivity in control and lesion groups of FPC animals was achieved by repeating this MDS analysis for experimental observation (animal for FPC-control, FPC-lesion). Dissimilarity matrices were calculated for every subject in both the FPC-control and FPC-lesion animals, before classical MDS was used to generate x/y coordinates for each ROI. To allow comparison across subjects/sessions, the coordinates calculated from each dissimilarity matrix in these FPC groups were aligned to the average MDS of FPC-control group (i.e. FPC reference). Alignment involved two steps: firstly in the calculated FPC-reference, x/y locations for each ROI were used as starting points for the MDS computation; secondly, a Procrustes transformation was used to align the x/y coordinates of each ROI to the reference locations for each subject in FPC groups separately (Kietzmann et al., 2019).

Changes in the average connectivity between the previously identified clusters was quantified by calculating the Euclidean distance between the centroid locations of each of the clusters. For each subject/session in the control and lesion groups of FPC, the Euclidean distance between these centroids was calculated and the resultant distances used in a within/between repeated measures ANOVA. This ANOVA had one within-subjects factor; Cluster (pairwise comparisons of the distance between the centroids of clusters) and one between-subjects factor; Lesion (control and lesion).

To confirm that lesion of PS did not affect the FPC-specific ROI network. This process was repeated in the PS-control and PS-lesion groups. As described above dissimilarity matrices were calculated for every subject in both the PS lesion groups, before classical MDS was used to generate x/y coordinates for each FPC-specific ROI. To allow comparison across subjects/sessions, the coordinates calculated from each dissimilarity matrix from both the PS groups were aligned to the average MDS of PS-control group (i.e. PS reference). Changes in connectivity between clusters in the PS-control and PS-lesion groups were then examined as described above.

4.9. Core vs. peripheral FPC network definition

To examine the anatomical and functional connections underlying the organisation of the FPC-specific network we conducted two analyses. Firstly, we identified core ROIs by applying a threshold to the network of functional connections. This threshold selected only the strongest 3 connections of each ROI. Prior to further analysis a number of thresholds were tested. Core ROIs were identified reliably with thresholds from 1 to 6 connections per ROI. However, when more connections were included hub identification failed (Figure S6). The threshold of 3 connections per ROI was selected as it fell within the midpoint of this range, and avoid under-sampling the connectivity matrices (Figure S6). We then calculated the degree centrality, defined as the sum of all connections, for each ROI in this thresholded network (Rubinov and Sporns, 2010). The

degree centrality for each ROI was compared to chance level, using a surrogate dataset in which connections were randomly shuffled. This bootstrap procedure was repeated 1000 times before statistical testing.

Comparison between the strength of FPC-specific ROIs function and anatomical connections to FPC was made using data made freely available by Markov (Markov et al. (2014)). As the brain parcellation methods used in our study (a finer LV-FOA-PHT composite atlas) and in Markov's study (based on a combination of their histological criteria (Markov et al., 2011) and atlas-based landmarks (Saleem and Logothetis, 2007) when necessary we have used the same single value to represent anatomical connection strength for several sub-divisions (for example using the FLNE value for area 23 to represent the connectivity for all sub-divisions of area 23).

Code Availability

The MATLAB code used to carry out these analyses and create the figures in this article are available from https://github.com/mainsworthxpsy/FPC_Lesion.

CRediT authorship contribution statement

*M.A and Z.W contributed equally and are joint first authors. M.J.B., H.B., Z.W., and M.A. conceived the project; M.J.B. supervised the project; Z.W. and M.A. performed the analyses; Z.W. and M.A. and M.J.B. interpreted the data and wrote the paper; A.H.B. helped implement MRI data-acquisition and MRI data-processing; A.H.B. and A.S.M. reviewed and commented upon the final draft manuscript; M.A., Z.W., H.B., A.S.M., A.H.B., and M.J.B. contributed technical and practical support to the conducting of the research.

Competing interests

The authors declare no financial or non-financial competing interests.

Data Availability

The connectivity matrices from all animals used in this study are available from https://github.com/mainsworthxpsy/FPC_Lesion.

Acknowledgements

Research and analyses primarily supported by the Biotechnology and Biological Sciences Research Council (BB/T00598X/1), Wellcome Trust, (WT101092MA), and Medical Research Council (MR/K005480/1). Additional support was provided by the Medical Research Council Intramural Program (SUAG/051 G101400) as well as the Wellcome Trust (110157/Z/15/Z) and Medical Research Council (G0800329). We thank G. Daubney for histological support. We thank lab members past and present for technical support, and we thank Oxford Biomedical Sciences team of expert animal technicians, veterinary staff, and anaesthetists for their very high standards of animal care and husbandry throughout.

Appendix A. Supporting information

Supplementary data associated with this article can be found in the online version at [doi:10.1016/j.pneurobio.2022.102314](https://doi.org/10.1016/j.pneurobio.2022.102314).

References

Adam, R., Johnston, K., Menon, R.S., Everling, S., 2020. Functional reorganization during the recovery of contralesional target selection deficits after prefrontal cortex lesions in macaque monkeys. *NeuroImage* 207, 116339. <https://doi.org/10.1016/j.neuroimage.2019.116339>.

- Ainsworth, M., Browncross, H., Mitchell, D.J., Mitchell, A.S., Passingham, R.E., Buckley, M.J., Duncan, J., Bell, A.H., 2018. Functional reorganisation and recovery following cortical lesions: a preliminary study in macaque monkeys. *Neuropsychologia* 119, 382–391. <https://doi.org/10.1016/j.neuropsychologia.2018.08.024>.
- Ainsworth, M., Sallet, J., Joly, O., Kyriazis, D., Kriegeskorte, N., Duncan, J., Schüffelen, U., Rushworth, M.F.S., Bell, A.H., 2021. Viewing ambiguous social interactions increases functional connectivity between frontal and temporal nodes of the social brain. *J. Neurosci.* 41, 6070–6086. <https://doi.org/10.1523/JNEUROSCI.0870-20.2021>.
- Badre, D., Wagner, A.D., 2004. Selection, integration, and conflict monitoring. *Neuron* 41, 473–487. [https://doi.org/10.1016/S0896-6273\(03\)00851-1](https://doi.org/10.1016/S0896-6273(03)00851-1).
- Behzadi, Y., Restom, K., Liu, J., Liu, T.T., 2007. A component based noise correction method (CompCor) for BOLD and perfusion based fMRI. *NeuroImage* 37, 90–101.
- Boorman, E.D., Behrens, T.E.J., Woolrich, M.W., Rushworth, M.F.S., 2009. How green is the grass on the other side? Frontopolar cortex and the evidence in favor of alternative courses of action. *Neuron* 62, 733–743. <https://doi.org/10.1016/j.neuron.2009.05.014>.
- Boschin, E.A., Buckley, M.J., 2015. Differential contributions of dorsolateral and frontopolar cortices to working memory processes in the primate. *Front. Syst. Neurosci.* 9, 1–8. <https://doi.org/10.3389/fnsys.2015.00144>.
- Boschin, E.A., Piekema, C., Buckley, M.J., 2015. Essential functions of primate frontopolar cortex in cognition. *Proc. Natl. Acad. Sci. U.S.A.* 112, E1020–E1027. <https://doi.org/10.1073/pnas.1419649112>.
- Buckley, M.J., Mansouri, F.A., Hoda, H., Mahboubi, M., Browning, P.G.F., Kwok, S.C., Phillips, A., Tanaka, K., 2009. Dissociable components of rule-guided behavior depend on distinct medial and prefrontal regions. *Science* 325, 52–58. <https://doi.org/10.1126/science.1172377>.
- Bunge, S.A., Helskog, E.H., Wendelken, C., 2009. Left, but not right, rostrolateral prefrontal cortex meets a stringent test of the relational integration hypothesis. *NeuroImage* 46, 338–342. <https://doi.org/10.1016/j.neuroimage.2009.01.064>.
- Burgess, P.W., Gonen-Yaacovi, G., Volle, E., 2011. Functional neuroimaging studies of prospective memory: what have we learnt so far. *Neuropsychologia* 49, 2246–2257. <https://doi.org/10.1016/j.neuropsychologia.2011.02.014>.
- Chen, O.Y., Cao, H., Reinen, J.M., Qian, T., Gou, J., Phan, H., de Vos, M., Cannon, T.D., 2019. Resting-state brain information flow predicts cognitive flexibility in humans. *Sci. Rep.* 9, 1–16. <https://doi.org/10.1038/s41598-019-40345-8>.
- Christoff, K., Prabhakaran, V., Dorfman, J., Zhao, Z., Kroger, J.K., Holyoak, K.J., Gabrieli, J.D.E., 2001. Rostrolateral prefrontal cortex involvement in relational integration during reasoning. *NeuroImage* 14, 1136–1149. <https://doi.org/10.1006/nimg.2001.0922>.
- Christoff, K., Ream, J.M., Geddes, L.P.T., Gabrieli, J.D.E., 2003. Evaluating self-generated information: anterior prefrontal contributions to human cognition. *Behav. Neurosci.* 117, 1161–1168. <https://doi.org/10.1037/0735-7044.117.6.1161>.
- Corbetta, M., 1998. Frontoparietal cortical networks for directing attention and the eye to visual locations: identical, independent, or overlapping neural systems? *Proc. Natl. Acad. Sci. U.S.A.* 95, 831–838. <https://doi.org/10.1073/pnas.95.3.831>.
- Corbetta, M., Shulman, G.L., 2002. Control of goal-directed and stimulus-driven attention in the brain. *Nat. Rev. Neurosci.* 3, 201–215. <https://doi.org/10.1038/nrn755>.
- Cusack, R., Vicente-Grabovetsky, A., Mitchell, D.J., Wild, C.J., Auer, T., Linke, A.C., Peelle, J.E., 2015. Automatic analysis (aa): efficient neuroimaging workflows and parallel processing using Matlab and XML. *Front. Neuroinformatics* 8, 1–13. <https://doi.org/10.3389/fninf.2014.00090>.
- Dal Monte, O., Chu, C.C.J., Fagan, N.A., Chang, S.W.C., 2020. Specialized medial prefrontal-amygdala coordination in other-regarding decision preference. *Nat. Neurosci.* 23, 565–574. <https://doi.org/10.1038/s41593-020-0593-y>.
- Daw, N.D., O'Doherty, J.P., Dayan, P., Seymour, B., Dolan, R.J., 2006. Cortical substrates for exploratory decisions in humans. *Nature* 441, 876–879. <https://doi.org/10.1038/nature04766>.
- Duncan, J., 2010. The multiple-demand (MD) system of the primate brain: mental programs for intelligent behaviour. *Trends Cogn. Sci.* 14, 172–179. <https://doi.org/10.1016/j.tics.2010.01.004>.
- Ercsey-Ravasz, M., Markov, N.T., Lamy, C., VanEssen, D.C., Knoblauch, K., Toroczkai, Z., Kennedy, H., 2013. A predictive network model of cerebral cortical connectivity based on a distance rule. *Neuron* 80, 184–197. <https://doi.org/10.1016/j.neuron.2013.07.036>.
- Essen, D.C. van, 2012. NeuroImage cortical cartography and caret software. *NeuroImage* 62, 757–764. <https://doi.org/10.1016/j.neuroimage.2011.10.077>.
- Fedorenko, E., Duncan, J., Kanwisher, N., 2013. Broad domain generality in focal regions of frontal and parietal cortex. *Proc. Natl. Acad. Sci. U.S.A.* 110, 16616–16621. <https://doi.org/10.1073/pnas.1315235110>.
- Finn, E.S., Shen, X., Scheinost, D., Rosenberg, M.D., Huang, J., Chun, M.M., Papademetris, X., Constable, R.T., 2015. Functional connectome fingerprinting: Identifying individuals using patterns of brain connectivity. *Nat. Neurosci.* 18, 1664–1671. <https://doi.org/10.1038/nn.4135>.
- Honey, C.J., Kötter, R., Breakspear, M., Sporns, O., 2007. Network structure of cerebral cortex shapes functional connectivity on multiple time scales. *Proc. Natl. Acad. Sci. U.S.A.* 104, 10240–10245. <https://doi.org/10.1073/pnas.0701519104>.
- Honey, C.J., Sporns, O., Cammoun, L., Gigandet, X., Thiran, J.P., Meuli, R., Hagmann, P., 2009. Predicting human resting-state functional connectivity from structural connectivity. *Proc. Natl. Acad. Sci. U.S.A.* 106, 2035–2040. <https://doi.org/10.1073/pnas.0811168106>.
- Hutchison, R.M., Hutchison, M., Manning, K.Y., Menon, R.S., Everling, S., 2014. Isoflurane induces dose-dependent alterations in the cortical connectivity profiles

- and dynamic properties of the brain's functional architecture. *Hum. Brain Mapp.* 35, 5754–5775. <https://doi.org/10.1002/hbm.22583>.
- Hutchison, R.M., Leung, L.S., Mirsattari, S.M., Gati, J.S., Menon, R.S., Everling, S., 2011. Resting-state networks in the macaque at 7T. *NeuroImage* 56, 1546–1555. <https://doi.org/10.1016/j.neuroimage.2011.02.063>.
- Hutchison, R.M., Mirsattari, S.M., Jones, C.K., Gati, J.S., Leung, L.S., 2010. Functional networks in the anesthetized rat brain revealed by independent component analysis of resting-state fMRI. *J. Neurophysiol.* 103, 3398–3406. <https://doi.org/10.1152/jn.00141.2010>.
- Kietzmann, T.C., Spoerer, C.J., Sörensen, L.K.A., Cichy, R.M., Hauk, O., Kriegeskorte, N., 2019. Recurrence is required to capture the representational dynamics of the human visual system. *Proc. Natl. Acad. Sci. U.S.A.* 116, 21854–21863. <https://doi.org/10.1073/pnas.1905544116>.
- Koechlin, E., Basso, G., Pietrini, P., Panzer, S., Grafman, J., 1999. The role of the anterior prefrontal cortex in human cognition. *Nature* 399, 148–151. <https://doi.org/10.1038/20178>.
- Koechlin, E., Corrado, G., Pietrini, P., Grafman, J., 2000. Dissociating the role of the medial and lateral anterior prefrontal cortex in human planning. *Proc. Natl. Acad. Sci. U.S.A.* 97, 7651–7656. <https://doi.org/10.1073/pnas.130177397>.
- Kwok, S.C., Cai, Y., Buckley, M.J., 2019. Mnemonic introspection in macaques is dependent on superior dorsolateral prefrontal cortex but not orbitofrontal cortex. *J. Neurosci.* 39, 5922–5934. <https://doi.org/10.1523/JNEUROSCI.0330-19.2019>.
- Mansouri, F.A., Buckley, M.J., Fehring, D.J., Tanaka, K., 2019. The role of primate prefrontal cortex in bias and shift between visual dimensions. *Cereb. Cortex* 1–15. <https://doi.org/10.1093/cercor/bhz072>.
- Mansouri, F.A., Buckley, M.J., Mahboubi, M., Tanaka, K., 2015. Behavioral consequences of selective damage to frontal pole and posterior cingulate cortices. *Proc. Natl. Acad. Sci. U.S.A.* 112, E3940–E3949. <https://doi.org/10.1073/pnas.1422629112>.
- Mansouri, F.A., Koechlin, E., Rosa, M.G.P., Buckley, M.J., 2017. Managing competing goals - a key role for the frontopolar cortex. *Nat. Rev. Neurosci.* 18, 645–657. <https://doi.org/10.1038/nrn.2017.111>.
- Mantini, D., Gerits, A., Nelissen, K., Durand, J.B., Joly, O., Simone, L., Sawamura, H., Wardak, C., Orban, G.A., Buckner, R.L., Vanduffel, W., 2011. Default mode of brain function in monkeys. *J. Neurosci.* 31, 12954–12962. <https://doi.org/10.1523/JNEUROSCI.2318-11.2011>.
- Markov, N.T., Ercsey-Ravasz, M.M., Ribeiro Gomes, A.R., Lamy, C., Magrou, L., Vezoli, J., Misery, P., Falchier, A., Quilodran, R., Gariel, M.A., Sallet, J., Gamanut, R., Huissoud, C., Clavagnier, S., Giroud, P., Sappey-Mariniér, D., Barone, P., Dehay, C., Toroczka, Z., Knoblauch, K., van Essen, D.C., Kennedy, H., 2014. A weighted and directed interareal connectivity matrix for macaque cerebral cortex. *Cereb. Cortex* 24, 17–36. <https://doi.org/10.1093/cercor/bhs270>.
- Markov, N.T., Misery, P., Falchier, A., Lamy, C., Vezoli, J., Quilodran, R., Gariel, M.A., Giroud, P., Ercsey-Ravasz, M., Pilaz, L.J., Huissoud, C., Barone, P., Dehay, C., Toroczka, Z., van Essen, D.C., Kennedy, H., Knoblauch, K., 2011. Weight consistency specifies regularities of macaque cortical networks. *Cereb. Cortex* 21, 1254–1272. <https://doi.org/10.1093/cercor/bhq201>.
- Mars, R.B., Jbabdi, S., Sallet, J., O'Reilly, J.X., Croxson, P.L., Olivier, E., Noonan, M.A.P., Bergmann, C., Mitchell, A.S., Baxter, M.G., Behrens, T.E.J., Johansen-Berg, H., Tomassini, V., Miller, K.L., Rushworth, M.F.S., 2011. Diffusion-weighted imaging tractography-based parcellation of the human parietal cortex and comparison with human and macaque resting-state functional connectivity. *J. Neurosci.* 31, 4087–4100. <https://doi.org/10.1523/JNEUROSCI.5102-10.2011>.
- McLaren, D.G., Kosmatka, K.J., Oakes, T.R., Kroenke, C.D., Kohama, S.G., Matochik, J.A., Ingram, D.K., Johnson, S.C., 2009. A population-average MRI-based atlas collection of the rhesus macaque. *NeuroImage* 45, 52–59. <https://doi.org/10.1016/j.neuroimage.2008.10.058>.
- Milham, M.P., Ai, L., Koo, B., Xu, T., Amiez, C., Balezeau, F., Baxter, M.G., Blezer, E.L.A., Brochier, T., Chen, A., Croxson, P.L., Damatac, C.G., Dehaene, S., Everling, S., Fair, D.A., Fleysher, L., Freiwald, W., Froudist-Walsh, S., Griffiths, T.D., Guedj, C., Hadj-Bouziane, F., ben Hamed, S., Harel, N., Hiba, B., Jarraia, B., Jung, B., Kastner, S., Klink, P.C., Kwok, S.C., Laland, K.N., Leopold, D.A., Lindenfors, P., Mars, R.B., Menon, R.S., Messinger, A., Meunier, M., Mok, K., Morrison, J.H., Nacef, J., Nagy, J., Rios, M.O., Petkov, C.I., Pinsk, M., Poirier, C., Procyk, E., Rajimehr, R., Reader, S.M., Roelfsema, P.R., Rudko, D.A., Rushworth, M.F.S., Russ, B.E., Sallet, J., Schmid, M.C., Schwiedrzik, C.M., Seidlitz, J., Sein, J., Shmuel, A., Sullivan, E.L., Ungerleider, L., Thiele, A., Todorov, O.S., Tsao, D., Wang, Z., Wilson, C.R.E., Yacoub, E., Ye, F.Q., Zarco, W., Zhou, Y., di Margulies, D.S., Schroeder, C.E., 2018. An open resource for non-human primate imaging. *e2 Neuron* 100, 61–74. <https://doi.org/10.1016/j.neuron.2018.08.039>.
- Mitchell, D.J., Bell, A.H., Buckley, M.J., Mitchell, A.S., Sallet, J., Duncan, J., 2016. A putative multiple-demand system in the macaque brain. *J. Neurosci.* 36, 8574–8585. <https://doi.org/10.1523/JNEUROSCI.0810-16.2016>.
- Nee, D.E., D'Esposito, M., 2017. Causal evidence for lateral prefrontal cortex dynamics supporting cognitive control. *eLife* 6, 1–19. <https://doi.org/10.7554/eLife.28040>.
- Nee, D.E., D'Esposito, M., 2016. The hierarchical organization of the lateral prefrontal cortex. *eLife* 5, 1–26. <https://doi.org/10.7554/eLife.12112>.
- Neubert, F., Mars, R.B., Sallet, J., Rushworth, M.F.S., 2015. Connectivity reveals relationship of brain areas for reward-guided learning and decision making in human and monkey frontal cortex. *Proc. Natl. Acad. Sci. U.S.A.* 112, E2695–E2704. <https://doi.org/10.1073/pnas.1410767112>.
- Neubert, F.X., Mars, R.B., Thomas, A.G., Sallet, J., Rushworth, M.F.S., 2014. Comparison of human ventral frontal cortex areas for cognitive control and language with areas in monkey frontal cortex. *Neuron* 81, 700–713. <https://doi.org/10.1016/j.neuron.2013.11.012>.
- Nichols, T.E., Holmes, A.P., 2001. Nonparametric permutation tests for functional neuroimaging: a primer with examples. *Hum. Brain Mapp.* 15, 1–25. <https://doi.org/10.1002/hbm.1058>.
- Nobre, A., 1997. Functional localization of the system for visuospatial attention using positron emission tomography. *Brain* 120, 515–533. <https://doi.org/10.1093/brain/120.3.515>.
- Okuda, J., Fujii, T., Ohtake, H., Tsukiura, T., Tanji, K., Suzuki, K., Kawashima, R., Fukuda, H., Itoh, M., Yamadori, A., 2003. Thinking of the future and past: the roles of the frontal pole and the medial temporal lobes. *NeuroImage* 19, 1369–1380. [https://doi.org/10.1016/S1053-8119\(03\)00179-4](https://doi.org/10.1016/S1053-8119(03)00179-4).
- Okuda, J., Fujii, T., Ohtake, H., Tsukiura, T., Yamadori, A., Frith, C.D., Burgess, P.W., 2007. Differential involvement of regions of rostral prefrontal cortex (Brodmann area 10) in time- and event-based prospective memory. *Int. J. Psychophysiol.* 64, 233–246. <https://doi.org/10.1016/j.ijpsycho.2006.09.009>.
- O'Reilly, J.X., Croxson, P.L., Jbabdi, S., Sallet, J., Noonan, M.P., Mars, R.B., Browning, P.G.F., Wilson, C.R.E., Mitchell, A.S., Miller, K.L., Rushworth, M.F.S., Baxter, M.G., 2013. Causal effect of disconnection lesions on interhemispheric functional connectivity in rhesus monkeys. *Proc. Natl. Acad. Sci. U.S.A.* 110, 13982–13987. <https://doi.org/10.1073/pnas.1305062110>.
- Passingham, R.E., Stephan, K.E., Köster, R., 2002. The anatomical basis of functional localization in the cortex. *Nat. Rev. Neurosci.* 3, 606–616. <https://doi.org/10.1038/nrn893>.
- Peleanos, V., Premereur, E., Mitchell, D.J., Chakraborty, S., Mason, S., Lee, A.C.H., Mitchell, A.S., 2020. Corticocortical and thalamocortical changes in functional connectivity and white matter structural integrity after reward-guided learning of visuospatial discriminations in Rhesus monkeys. *J. Neurosci.* 40, 7887–7901. <https://doi.org/10.1523/JNEUROSCI.0364-20.2020>.
- Peltier, S.J., Kerssens, C., Hamann, S.B., Sebel, P.S., Byas-Smith, M., Hu, X., 2005. Functional connectivity changes with concentration of sevoflurane anesthesia. *NeuroReport* 16, 285–288. <https://doi.org/10.1097/00001756-200502280-00017>.
- Petrides, M., Pandya, D.N., 2007. Efferent association pathways from the rostral prefrontal cortex in the macaque monkey. *J. Neurosci.* 27, 11573–11586. <https://doi.org/10.1523/JNEUROSCI.2419-07.2007>.
- Raichle, M.E., MacLeod, A.M., Snyder, A.Z., Powers, W.J., Gusnard, D.A., Shulman, G.L., 2001. A default mode of brain function. *Proc. Natl. Acad. Sci. U.S.A.* 98, 676–682. <https://doi.org/10.1073/pnas.98.2.676>.
- Rubinov, M., Sporns, O., 2010. Complex network measures of brain connectivity: Uses and interpretations. *NeuroImage* 52, 1059–1069. <https://doi.org/10.1016/j.neuroimage.2009.10.003>.
- Rudebeck, P.H., Saunders, R.C., Prescott, A.T., Chau, L.S., Murray, E.A., 2013. Prefrontal mechanisms of behavioral flexibility, emotion regulation and value updating. *Nat. Neurosci.* 16, 1140–1145. <https://doi.org/10.1038/nn.3440>.
- Ryals, A.J., Wang, J.X., Polnaszek, K.L., Voss, J.L., 2015. Hippocampal contribution to implicit configuration memory expressed via eye movements during scene exploration. *Hippocampus* 25, 1028–1041. <https://doi.org/10.1002/hipo.22425>.
- Sakai, K., Passingham, R.E., 2006. Prefrontal set activity predicts rule-specific neural processing during subsequent cognitive performance. *J. Neurosci.* 26, 1211–1218. <https://doi.org/10.1523/JNEUROSCI.3887-05.2006>.
- Saleem, K.S., Logothetis, N., 2012. A combined MRI and histology atlas of the rhesus monkey brain in stereotaxic coordinates.
- Saleem, K.S., Logothetis, N.K., 2007. A combined MRI and histology atlas of the rhesus monkey brain in stereotaxic coordinates.
- Saleem, K.S., Miller, B., Price, J.L., 2014. Subdivisions and connective networks of the lateral prefrontal cortex in the macaque monkey. *J. Comp. Neurol.* 522, 1641–1690. <https://doi.org/10.1002/cne.23498>.
- Schmahmann, J.D., Pandya, D.N., 2006. *Fiber Pathways of the Brain*. Oxford University Press.
- Sliwa, J., Freiwald, W.A., 2017. A dedicated network for social interaction processing in the primate brain. *Science* 356, 745–749. <https://doi.org/10.1126/science.aam6383>.
- van Essen, D.C., Glasser, M.F., Dierker, D.L., Harwell, J., 2012. Cortical parcellations of the macaque monkey analyzed on surface-based atlases. *Cereb. Cortex* 22, 2227–2240. <https://doi.org/10.1093/cercor/bhr290>.
- Vezoli, J., Vinck, M., Bosman, C.A., Bastos, A.M., Lewis, C.M., Kennedy, H., Fries, P., 2021. Brain rhythms define distinct interaction networks with differential dependence on anatomy. *Neuron* 3862–3878. <https://doi.org/10.1016/j.neuron.2021.09.052>.
- Vincent, J.L., Patel, G.H., Fox, M.D., Snyder, A.Z., Baker, J.T., van Essen, D.C., Zempel, J.M., Snyder, L.H., Corbetta, M., Raichle, M.E., 2007. Intrinsic functional architecture in the anesthetized monkey brain. *Nature* 447, 83–86. <https://doi.org/10.1038/nature05758>.
- Voytek, B., Davis, M., Yago, E., Barceló, F., Vogel, E.K., Knight, R.T., 2010. Dynamic Neuroplasticity after Human Prefrontal Cortex Damage. *Neuron* 68, 401–408. <https://doi.org/10.1016/j.neuron.2010.09.018>.
- Yokoyama, O., Miura, N., Watanabe, J., Takemoto, A., Uchida, S., Sugiyama, M., Horie, K., Sato, S., Kawashima, R., Nakamura, K., 2010. Right frontopolar cortex activity correlates with reliability of retrospective rating of confidence in short-term recognition memory performance. *Neurosci. Res.* 68, 199–206. <https://doi.org/10.1016/j.neures.2010.07.2041>.
- Zajkowski, W.K., Kossut, M., Wilson, R.C., 2017. A causal role for right frontopolar cortex in directed, but not random, exploration. *eLife* 6, 1–18. <https://doi.org/10.7554/eLife.27430>.